https://doi.org/10.5194/egusphere-2025-1495
Preprint. Discussion started: 14 April 2025

Interactions between ocean alkalinity enhancement and phytoplankton in an Earth System Model

Miriam Seifert[1], Christopher Danek[1], Christoph Völker[1], and Judith Hauck[1,2]

[1]Alfred-Wegener-Institut Helmholtz-Zentrum für Polar- und Meeresforschung, 27570 Bremerhaven, Germany
[2]Universität Bremen, 28359 Bremen, Germany

Correspondence: Miriam Seifert (miriam.seifert@awi.de)

Abstract. Ocean alkalinity enhancement (OAE) as a CO_2 removal strategy is well investigated in model studies, but risks for the ecosystem are presently not considered in models. Our study examines OAE-phytoplankton feedbacks in an Earth System Model by adding carbonate system dependencies to the phytoplankton growth term. OAE is performed between 2040 and 2100 in the exclusive economic zones of Europe, the US, and China, with alkalinity additions reaching 103.2 Tmol year^{-1} by the end of the century. Atmospheric pCO_2 is reduced by 3−8 μatm. The excess ocean CO_2 sink is mainly chemically driven, but can additionally be altered by biological feedbacks. Further, net primary production decreases by up to 15% due to indirect effects of OAE. Our results do not confirm the direct positive effect of OAE on calcifying coccolithophores. Limiting alkalinity addition in locations with high aragonite saturation states is beneficial as it not only reduces the OAE impact on phytoplankton but also increases the reduction in atmospheric pCO_2. Our study highlights the need to take ecosystem responses into account when evaluating the effectiveness of OAE.

1 Introduction

In order to limit global warming to well below 2°C above preindustrial levels by 2100 as strived for in the Paris Agreement (UNFCCC, 2015), rapid phasing out of fossil fuels is required (Ho, 2023; Oschlies et al., 2023). However, to offset residual or hard-to-abate emissions such as carbon dioxide (CO_2) emissions from aviation and maritime transport as well as non-CO_2 greenhouse gas emissions from agriculture (Oschlies et al., 2023; Ho, 2023), a portfolio of different carbon dioxide removal (CDR) technologies would require to sequester about 6−10 Gt atmospheric CO_2 per year (equivalent to 1.6−2.7 Pg C year^{-1}, Smith et al., 2024). Indeed, all scenarios of the 6th report of the Intergovernmental Panel on Climate Change (IPCC) that limit warming to 1.5−2°C above preindustrial levels assume CDR implementation (Buck et al., 2023; Smith et al., 2024). Because terrestrial CDR technologies are often limited by competition for area (Fuss et al., 2014; Boysen et al., 2017; Friedlingstein et al., 2019), efforts increasingly focus on marine CDR technologies. One of the most promising ocean-based approaches is ocean alkalinity enhancement (OAE, Köhler et al., 2013; Burns and Corbett, 2020; Gattuso et al., 2021).

The concept of OAE is to shift the ocean carbonate equilibria by adding alkaline substrates to the water. Simplified, total alkalinity quantifies carbonate and bicarbonate ion charges in the ocean (Zeebe and Wolf-Gladrow, 2001). Increasing alkalinity

https://doi.org/10.5194/egusphere-2025-1495
Preprint. Discussion started: 14 April 2025

initially raises the *p*H of seawater, shifts the carbonate chemistry speciation towards lower aqueous CO_2 and higher carbonate ion concentration, and increases the saturation state of calcium carbonate ($CaCO_3$). Ultimately, this allows additional atmospheric CO_2 to dissolve in seawater and be stored as bicarbonate or carbonate ions. Natural rock weathering, for example, sequesters about 0.14 Pg C year^{-1} (Renforth and Henderson, 2017). OAE efforts aim to mimic this natural process by actively deploying natural or artificially produced alkaline material to the surface ocean (Renforth and Henderson, 2017; Caserini et al., 2022). One of the possible alkalinity sources is calcium oxide or quicklime (CaO), which can be derived from limestone (a raw material for cement production) in a chemical process (Stanmore and Gilot, 2005; Caserini et al., 2022; Foteinis et al., 2022). In comparison to other alkaline material such as olivine and basalt, CaO shows rapid near-surface dissolution (Fakhraee et al., 2023), enabling atmospheric CO_2 uptake by the ocean, which would not occur if dissolution happened at depth.

The main limitations of OAE are limited feedstock supply, CO_2 emissions during the production of the OAE substrate (Fakhraee et al., 2023) and secondary precipitation of $CaCO_3$ that can remove more alkalinity than was added (Moras et al., 2022; Schulz et al., 2023). Nonetheless, there is no doubt that in principle adding alkalinity can indeed be an efficient CDR method as shown by numerous model studies (e.g., Hauck et al., 2016; Feng et al., 2017; Butenschön et al., 2021; Palmiéri and Yool, 2024). A major gap in the current models assessing the efficiency of OAE is, however, the disregard of feedbacks between OAE and the ocean planktonic ecosystem, although it was identified as a major risk (Fennel et al., 2023).

The shift from CO_2 to bicarbonate and carbonate could potentially drive primary producers into CO_2 limitation, especially when the use of bicarbonate for photosynthesis is limited (Riebesell et al., 1993; Bach et al., 2019). In a review, Bach et al. (2019) argue that a transient shift in carbonate chemistry conditions should have little impact on the overall productivity. Indeed, there is minimal evidence for a harmful impact of enhanced alkalinity on the plankton community (Ramírez et al., 2024). Yet, changes in the phytoplankton species composition may be triggered, for example by a competitive advantage of small over large cells due to more efficient diffusion of CO_2 to the cell surface (Wolf-Gladrow and Riebesell, 1997; Chrachri et al., 2018; Bach et al., 2019). Bach et al. (2019) further hypothesize that calcifiers may become more important in regions of alkalinity deployment (change from "blue ocean" to "white ocean") due to carbonate chemistry conditions that are more favorable for calcification. In particular, this may hold under strong alkalinity enhancement, whereas weaker alkalinity addition could mainly counteract the negative impacts of ocean acidification on calcification (Lehmann and Bach, 2025). However, experimental studies show little to no effects of OAE on calcification (Subhas et al., 2022; Faucher et al., 2025; Bednaršek et al., 2025), especially as long as fluctuations in *p*H remain in a natural range (Gately et al., 2023), and partly even negative effects on the growth of calcifiers (Faucher et al., 2025). Furthermore, OAE was observed to have no (Gately et al., 2023) or a small negative effect (Ferderer et al., 2022) on silicification and has the potential to modify the carbon-to-nitrogen ratio (Ferderer et al., 2022). While the effects of OAE on calcifiers and silicifiers remain vague, Paul et al. (2024) show that increasing alkalinity can modify the nitrogen turnover, leading to a higher carbon-to-nitrogen ratio in particulate organic matter and ultimately to a decrease in the food quality.

https://doi.org/10.5194/egusphere-2025-1495
Preprint. Discussion started: 14 April 2025

In contrast to these uncertain effects of OAE on the ecosystem, calcification has a distinct effect on OAE. The formation of one mole $CaCO_3$ removes two moles of alkalinity - this so-called "leakage term" reduces the efficiency of OAE (Bach et al., 2019; Ho et al., 2003). In a modelling study, for example, the proliferation of calcifiers due to nutrient addition along with alkalinity, led to a decrease of surface alkalinity and hence OAE efficiency relative to a model simulation without nutrient addition (Nagwekar et al., 2024). Thus, changes in calcification rates and the distribution of calcifiers caused by OAE should be considered in modelling studies when accounting for atmospheric CO_2 removal through OAE. For the same reasons, abiotic calcium carbonate precipitation, triggered at high aragonite saturation states in high-alkaline environments, can reduce OAE efficiency (Suitner et al., 2024), but its implication for real-ocean OAE is still unknown (e.g., Hartmann et al., 2023).

Adressing a gap in the current OAE modelling approaches, our study investigates the link between large-scale OAE and the ocean ecosystem. In particular, we use an earth system model that links carbonate system changes to phytoplankton growth and calcification, and changes in calcification and calcite dissolution to the OAE efficiency. This allows an improved understanding of OAE effects in the living ocean.

2 Methods

2.1 AWI-ESM-1-REcoM

We computed emission-driven simulations with the Alfred Wegener Institute Earth System Model (AWI-ESM-1-REcoM). AWI-ESM is based on the AWI Climate Model (AWI-CM1, Semmler et al., 2020), but includes dynamic vegetation on land (Reick et al., 2021). AWI-ESM-1-REcoM further includes the representation of the carbon cycle between land, ocean, and atmosphere. Ocean and sea ice are represented by the Finite Element Sea Ice-Ocean Model FESOM (FESOM1.4, Danilov et al., 2004; Wang et al., 2014). Ocean biogeochemistry is described by the Regulated Ecosystem Model REcoM (REcoM2, Hauck et al., 2013; Schourup-Kristensen et al., 2014). The ocean and ocean biogeochemistry components are discretized on an unstructured mesh, allowing a variable grid resolution (12–147 km, mean 76 km, median 41 km). The carbonate system in REcoM is computed across the entire water column by the mocsy 2.0 routine (Orr and Epitalon, 2015; Seifert et al., 2022). The atmospheric component of AWI-ESM is represented by the spectral atmospheric model ECHAM (version 6.3, Stevens et al., 2013; Giorgetta et al., 2013). Land dynamics are modeled by the land surface model JSBACH version 3.20 including dynamic vegetation and the soil carbon model Yasso (Reick et al., 2021).

2.2 Modifications in REcoM for carbonate system effects on phytoplankton

The ocean biogeochemistry model REcoM describes the cycling of carbon, nitrogen, silicon, iron, and oxygen (Hauck et al., 2013). In the control version (without carbonate system effects, hereafter called "NO-CSE"), the ecosystem consists of two phytoplankton groups (small phytoplankton, diatoms), two zooplankton groups (generic zooplankton, polar macrozooplankton), and two detritus groups (slow and fast-sinking, Karakuş et al., 2021). Calcification is proportional to the gross photosynthesis

https://doi.org/10.5194/egusphere-2025-1495
Preprint. Discussion started: 14 April 2025

rate of 2% of the small phytoplankton group with a fixed particulate inorganic to organic carbon ratio $(\mathrm{PIC:POC})_{ref} = 1$. Calcite dissolution scales only with depth. Further, the 3D ocean carbonate system as well as the CO_2 flux between atmosphere and ocean is computed by the mocsy 2.0 routines (Orr and Epitalon, 2015). A more detailed description of REcoM can be found in Appendix A.

Deviating from this control version, three major code changes of REcoM were used in this study (further on called "CSE") as described in Seifert et al. (2022). Firstly, coccolithophores as a new group of explicitly calcifying phytoplankton were added to the ecosystem, replacing the fixed share of 2% calcifiers in the small phytoplankton group. Calcification in CSE is not only a function of the gross photosynthesis rate, but also dependent on temperature and dissolved inorganic nitrogen (DIN) limitation resulting in a variable PIC:POC ratio. Secondly, the CSE version accommodates for direct effects of OAE on calcification as well as on gross photosynthesis of all phytoplankton groups. Thirdly, the carbonate ion concentration, and not depth, determines the calcite dissolution.

To account for direct effects of alkalinity enhancement on phytoplankton, the gross photosynthesis and calcification functions in REcoM were supplemented by a CO_2 term $f(\mathrm{CO_2})$ that scales between zero and three (i.e., maximal three-fold increase of gross photosynthesis and calcification) depending on changes in the carbonate system. The term was initially developed to describe responses to ocean acidification (Bach et al., 2015; Seifert et al., 2022). As systematic assessments of OAE effects on phytoplankton growth and calcification are missing to date, we assumed that growth and calcification responses to changes in alkalinity can be described by the same function as responses to ocean acidification. Gross photosynthesis PS is defined as:

$$PS_i = f(T)_i \cdot f(PAR)_i \cdot f(\mathrm{N})_i \cdot f(\mathrm{CO_2})_i, \tag{1}$$

where $f(T)_i$, $f(PAR)_i$, and $f(\mathrm{N})_i$ describe the effects of temperature, photosynthetically active radiation (PAR) and nutrient availability on the gross photosynthesis rate PS_i of the phytoplankton functional group *i* (more details in Text S2). Calcification *Calc* of coccolithophores (denoted by *j*) is defined as:

$$Calc_j = PS_j \cdot C_j \cdot (\mathrm{PIC:POC})_{ref} \cdot f(T)_{j,calc} \cdot f(\mathrm{N})_{j,calc} \cdot f(\mathrm{CO_2})_{calc}, \tag{2}$$

where C_j is the biomass of coccolithophores and $(\mathrm{PIC:POC})_{ref}$ a reference PIC:POC ratio of one. The temperature and DIN dependencies of calcification, $f(T)_{j,calc}$ and $f(\mathrm{N})_{j,calc}$, follow Krumhardt et al. (2017). Calcification decreases linearly at temperatures below 10.6°C. The dependence on DIN limitation (modified from the original phosphate limitation, Krumhardt et al., 2017) is described by a modified Michaelis-Menten equation. Both terms are explained in more detail in Appendix B and C. The CO_2 factor $f(\mathrm{CO_2})$ in both parameterizations is defined as:

$$f(\mathrm{CO_2})_{i\ or\ calc} = \frac{a_i \cdot [\mathrm{HCO_3^-}]}{b_i + [\mathrm{HCO_3^-}]} - \exp(-c_i \cdot [\mathrm{CO_{2(aq)}}]) - d_i \cdot 10^{-p\mathrm{H}}. \tag{3}$$

The parameters *a*, *b*, *c*, and *d* (Table A1) were derived from curve fitting to experimental phytoplankton growth data Seifert et al. (2022), and $[\mathrm{HCO_3}^-]$, $[\mathrm{CO_2}(aq)]$, and *p*H are the concentrations of bicarbonate, dissolved CO_2 and *p*H in the surrounding

https://doi.org/10.5194/egusphere-2025-1495
Preprint. Discussion started: 14 April 2025

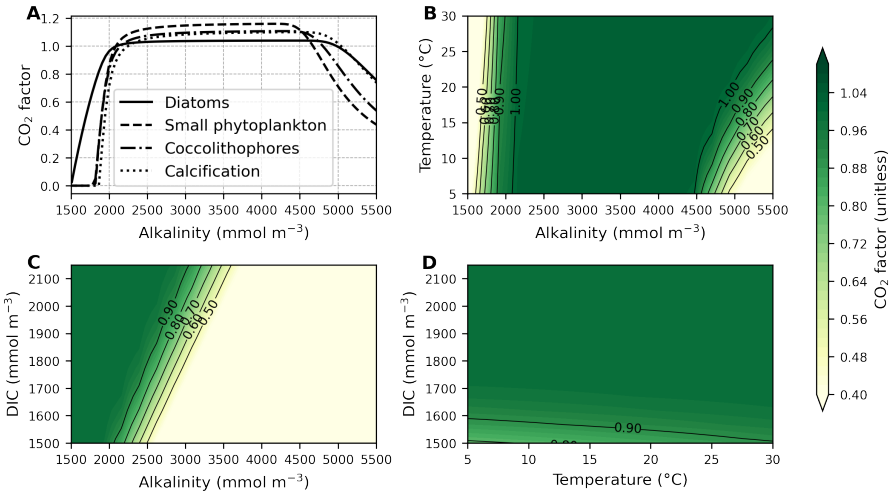

Figure 1. The CO_2 factor of phytoplankton net photosynthesis rate and calcification following Eq. 3. (A) displays variations in the factor with increasing alkalinity at surface pressure, a constant temperature of 20°C, salinity of 35, zero silicate and phosphate concentrations, and a DIC concentration of 1950 mmol m^{-3}. Contour plots show changes in the CO_2 factor of diatoms with (B) varying temperature, (C) varying DIC concentrations, and (D) both varying temperature and DIC concentrations at a constant alkalinity concentration of 2150 mmol m^{-3}. Carbonate system parameters for the plots were computed with PyCO2SYS version 1.8.3 (Humphreys et al., 2022).

seawater. The CO_2 factor is zero at low alkalinity (or low HCO_3^- concentrations), plateaus at medium alkalinity, and decreases at high alkalinity (or low $CO_2(aq)$ concentrations) (Fig. 1A). Low temperatures (Fig. 1B) and low concentrations of dissolved inorganic carbon (DIC; Fig. 1C) narrow the window of maximum CO_2 factor values. In turn, it is high at high temperature and DIC concentrations (Fig. 1D).

2.3 Model simulations

Model simulations for this study were branched off after an initial concentration-driven spinup (piControl) of 1051 years with a constant atmospheric CO_2 concentration of 278 ppm, and a subsequent emission-driven spinup (esm-piControl) of 871 years. Additional 200 years of esm-piControl spinup with both the NO-CSE and the CSE model version (section 2.2) were computed in parallel before starting the historical simulations (1850-2014; HIST-NO-CSE and HIST-CSE). For the subsequent future simulations, the SSP5-3.4-OS scenario was used. It follows the initial ramp-up of emissions equal to the SSP5-8.5 scenario (the unmitigated baseline scenario) from 2015 to 2039 before strong emission reduction from 2040 onwards, reaching zero emissions in 2070 and net negative emissions thereafter (O'Neill et al., 2016). Net negative emissions in this scenario are obtained by CDR methods other than OAE and additive to the OAE-caused atmospheric CO_2 reduction investigated in our study.

Starting in 2040 we added alkalinity with two different concentrations ("OAE-low", "OAE-high") in both model versions (section 2.4). We also computed simulations without alkalinity addition for each model version ("NO-OAE"). Hence, we

https://doi.org/10.5194/egusphere-2025-1495
Preprint. Discussion started: 14 April 2025

ended up with six simulations for 2040-2100: NO-CSE-NO-OAE, NO-CSE-OAE-low, NO-CSE-OAE-high, CSE-NO-OAE, CSE-OAE-low, CSE-OAE-high. Further, we computed one simulation which builds on the CSE-OAE-high simulation but in which no alkalinity was added to a grid cell when the saturation state of aragonite exceeded 10 to avoid conditions that favour abiotic calcium carbonate precipitation (CSE-OAE-high-lim). We analysed differences between CSE and NO-CSE simulations as well as between OAE-high / OAE-low and NO-OAE simulations with *t*-tests (significance level: 0.95) either for the entire time series 2040-2100 or for the last 10 years of the simulation (2091-2100).

2.4 OAE mask and alkalinity deployment

Alkalinity was added to the surface ocean in the exclusive economic zones (EEZ; up to 200 nautical miles away from the coastlines) of Europe, the US, and China (Fig. 2A). Subpolar regions (north of 67.5°N), the Baltic Sea east of 9.5°E as well as small marginal seas and remote parts of the EEZ (e.g., islands in the Pacific and Atlantic Ocean, Greenland) were excluded from the mask. The amount of alkalinity added in the OAE-high simulations scales according to the availability of CaO from cement production (Foteinis et al., 2022), with increasing annual cement production and, hence, CaO additions from 2040 to 2100 (Fig. 2B). In the OAE-low simulations half of this amount was added to the EEZ. Given the vast growth of the cement production in China over the past decades (S. Foteinis, personal communication), the Chinese EEZ starts with the highest alkalinity addition in the beginning of the deployment time and begins to saturate by the end of the century, while the amounts added to the European and the US EEZ progressively increase over time. In each grid cell of the model, the addition scales with the relative sea-ice cover which is assumed to prevent the distribution of alkalinity to the surface ocean. While the European and the Chinese EEZ are not affected by sea ice, the deployment in the US EEZ as reported here is 2.5±0.6% (2.7±1.3%) smaller in the first (last) decade of the deployment than in the initial deployment mask. In 2100, the amounts of alkalinity in the OAE-high (OAE-low) simulations are: Europe: 29.7 (14.9) Tmol year^{-1}; USA: 23.9 (12.1) Tmol year^{-1}; China: 49.6 (24.8) Tmol year^{-1}.

2.5 Analysis

The efficiency of OAE (ηCO_2) is computed from excess volume-integrated DIC and alkalinity in the OAE relative to the respective NO-OAE simulations (Renforth and Henderson, 2017) as:

$$\eta CO_2 = \frac{\Delta DIC}{\Delta Alkalinity}. \quad (4)$$

The reduction of the CO_2 partial pressure in seawater ($pCO_{2(aq)}$) due to biological carbon drawdown, $\Delta pCO_{2(aq,bio)}$, is computed based on the biological sources and sinks to DIC (ΔDIC_{bio}) as well as the surface ocean carbonate system averaged over the upper 100 m of the water column (Hauck and Völker, 2015; Oziel et al., 2025) with:

$$\Delta pCO_{2(aq,bio)} = \frac{\Delta DIC_{bio}}{\gamma_{DIC}} \cdot pCO_{2(aq)}. \quad (5)$$

The buffer factor $\gamma_{DIC} = \frac{DIC}{R}$ (Egleston et al., 2010), with R being the Revelle factor (ratio of the relative change in $pCO_{2(aq)}$ to the relative change in DIC, Zeebe and Wolf-Gladrow, 2001). Sources of DIC_{bio} are phytoplankton and zooplankton res-

https://doi.org/10.5194/egusphere-2025-1495
Preprint. Discussion started: 14 April 2025

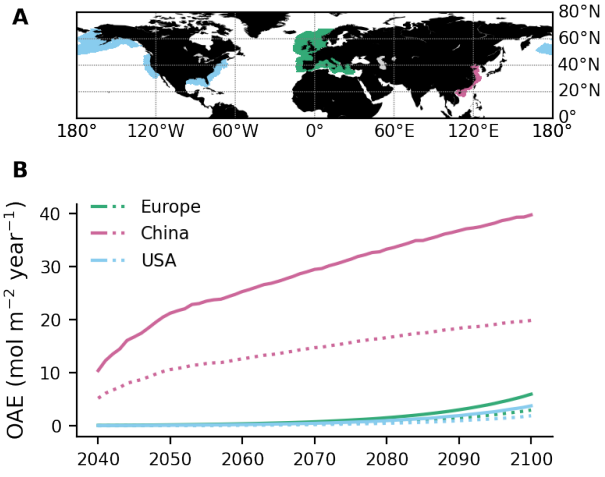

Figure 2. (A) Deployment regions along the European (green), Chinese (magenta), and the US EEZ (blue). (B) Amount of alkalinity added per m^{-2} annually between 2040 and 2100 in each deployment region (solid: OAE-high, dotted: OAE-low).

piration, $CaCO_3$ dissolution, and remineralization of dissolved organic carbon, while photosynthesis and calcification are sinks of DIC_{bio}. Due to its strong seasonality, $pCO_{2(aq,bio)}$ is calculated monthly and then averaged annually. Furthermore, $\Delta pCO_{2(aq,bio)}$ allows to artificially combine the effects of carbonate system states (buffer factor and $pCO_{2(aq)}$) and biological feedbacks of different simulations on the biological pCO_2 drawdown. Both measures, ηCO_2 and $\Delta pCO_{2(aq,biol)}$, are computed both for the global ocean and in the three deployment regions as mean over 2091-2100.

3 Results

3.1 OAE efficiency and modification by biological feedbacks

The reduction in atmospheric pCO_2 in the OAE-low and OAE-high simulations relative to the NO-OAE simulations ranges from 2.9 to 7.8 μatm (mean 2091-2100) and scales roughly with the amount of alkalinity added (Fig. 3A). Surface alkalinity (mean 2091-2100) in the OAE-high (OAE-low) simulation increases by 104−105 mmol m^{-3} (53−54 mmol m^{-3}) in the European EEZ, 100−106 mmol m^{-3} (50−52 mmol m^{-3}) in the US EEZ, and 619−649 mmol m^{-3} (313−321 mmol m^{-3}) in the Chinese EEZ (range given for CSE and NO-CSE simulations). Relative to the simulation without alkalinity addition (NO-OAE), this is an increase in surface alkalinity of 5−30% for OAE-high (2−15% for OAE-low). Globally, $pCO_{2(aq)}$ in the upper 100 m mainly follows the trajectory of the prescribed CO_2 emissions (increasing $pCO_{2(aq)}$ by about 60 μatm until 2060, decreasing $pCO_{2(aq)}$ thereafter), and differences between the CSE and the NO-CSE simulations without alkalinity addition are largely caused by the model setup (Fig. A1A). In the deployment regions, $pCO_{2(aq)}$ in the NO-OAE simulations is additionally modified by regional dynamics in the air-sea CO_2 fluxes (Fig. A1B−D). Furthermore, by 2100 the simulations differ according to the amount of alkalinity added, with highest $pCO_{2(aq)}$ values in the NO-OAE and lowest in the OAE-high simulations. Re-

https://doi.org/10.5194/egusphere-2025-1495
Preprint. Discussion started: 14 April 2025

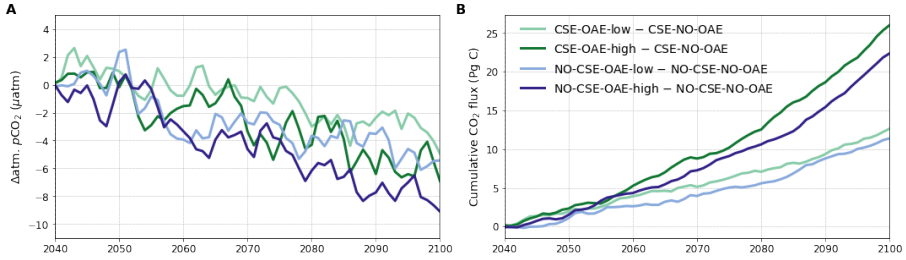

Figure 3. (A) Anomalies in atmospheric pCO_2 (negative = reduction) and (B) anomalies in the cumulative air-sea CO_2 flux (positive = into the ocean) in the OAE simulations relative to the NO-OAE simulations for the time period of alkalinity addition (2040-2100, annual means).

Table 1. Anomalies in atmospheric pCO_2 as well as cumulative air-sea and air-land CO_2 fluxes relative to the NO-OAE simulations. Negative sign for Δatm. pCO_2 represents a decrease in atmospheric pCO_2 concentration. Positive signs for the air-sea and air-land CO_2 fluxes indicate an increasing sink or decreasing source. Stars indicate significant differences to the respective NO-OAE simulations.

	Δatm. pCO_2 (μatm), mean 2091−2100	Δcum. air-sea CO_2 flux (Pg C), 2100	Δcum. air-land CO_2 flux (Pg C), 2100
CSE-OAE-low	−2.9	+12.6*	−0.5*
CSE-OAE-high	−5.7	+26.0*	−8.4*
NO-CSE-OAE-low	−5.0	+11.4*	+1.4
NO-CSE-OAE-high	−7.8*	+22.4*	−0.8*
CSE-OAE-high-lim	*−6.1*	*+23.8**	*−6.8**

ductions in near-surface air temperatures and sea surface temperatures relative to the NO-OAE simulations are non-significant. This is probably due to both the relatively small reduction in atmospheric pCO_2 that may not result in temperature changes that go beyond natural variability as well as the time lag in the Earth system response, in line with Jeltsch-Thömmes et al. (2024).

OAE causes a significant increase of the global cumulative air-sea CO_2 flux in all simulations, ranging between 11.4 and 26.0 Pg C by 2100 (Fig. 3B and A2, Table 1). About half of the OAE-induced CO_2 flux change occurs outside the deployment regions (Table 2). Including areas of 1000 km distance from the deployment region, resulting in areas that are 3−4 times the size of the original deployment regions (Fig. A3), covers 80−90% of the excess CO_2 uptake (Table A2). Especially in the US and the Chinese EEZ, a considerable share of excess ocean CO_2 uptake happens in the >1000 km surrounding area of the deployment region (Fig. 4A−C).

Within the deployment regions, OAE is least efficient in the Chinese EEZ (0.34−0.45) and most efficient in the US EEZ (0.65−0.88; Table 2). Efficiency in the Chinese EEZ increases when considering the surrounding 1000 km (0.55−0.67, Fig. 4F, Table A2). Conversely, the efficiency in the US EEZ decreases slightly until a distance of 1000 km vicinity, while the effi-

https://doi.org/10.5194/egusphere-2025-1495
Preprint. Discussion started: 14 April 2025

Table 2. Relative contribution of the deployment areas to anomalies in cumulative global air-sea CO_2 fluxes, and OAE efficiencies within the deployment regions. "Rest": global minus deployment regions; "Global": including deployment regions.

	Relative contribution to anomalies in air-sea CO_2 flux (%), 2100				OAE efficiency (ΔDIC / ΔAlkalinity), mean 2091-2100			
	Europe	USA	China	Rest	Europe	USA	China	Global
CSE-OAE-low	11.7	10.0	31.2	47.2	0.75	0.69	0.45	0.72
CSE-OAE-high	11.1	9.9	24.0	55.0	0.67	0.88	0.36	0.73
NO-CSE-OAE-low	13.0	10.2	33.5	43.2	0.55	0.76	0.42	0.66
NO-CSE-OAE-high	11.8	11.2	26.7	50.2	0.63	0.65	0.34	0.62

ciency in the European EEZ remains rather constant over the entire distance from the deployment region analysed here (Fig. 4D,E, Table A2). This can likely be explained by surface currents that transport the added alkalinity and thereby the enhanced CO_2 uptake out of the deployment region, in particular in the Chinese EEZ. Surface currents can also cause fluctuations in the efficiency with increasing distance from the deployment region by modifying the time in which alkalized waters are in contact with the atmosphere to take up additional atmospheric CO_2. In summary, these results highlight the different dynamics in the deployment regions: in our simulations, OAE works well or even best closest to the deployment regions of the European and the US EEZ, while the OAE effect in the Chinese EEZ is distributed over an area that is larger than the actual deployment region.

When accounting for carbonate system effects on phytoplankton, the ocean takes up $11-16\%$ more excess CO_2 than without these effects (Table 1). However, the reduction in atmospheric pCO_2 is smaller due to the weakened land CO_2 uptake (Table 1). The stronger CO_2 sink in the CSE simulations could solely be driven by lower initial alkalinity and DIC concentrations compared to the NO-CSE simulations (Fig. A4) which chemically favor the uptake of atmospheric CO_2. To identify whether carbonate system effects on phytoplankton play an additional role in enhancing the ocean CO_2 uptake in the CSE simulations, we computed $\Delta pCO_{2(aq,bio)}$ (Eq. 5).

The biological pCO_2 drawdown is a function of the strength of primary production and of the buffer capacity of seawater. Here, we combine results of different simulations to disentangle the roles of changing NPP in response to OAE and of different carbonate system states for the simulated ocean carbon uptake. The biological pCO_2 drawdown is consistently smaller in simulations with OAE than in those without, independent of whether carbonate system effects on phytoplankton growth are represented (about 20% in the European and US EEZ, about 60% in the Chinese EEZ, and about 3% globally; p-value<0.05, Fig. 5, Table A3). This is because OAE increases the buffer capacity and thus reduces the imprint of NPP on pCO_2 drawdown (Hauck and Völker, 2015). On top of that, two competing processes are responsible for differences between the CSE and NO-CSE simulations. Firstly, the CSE effects alter NPP and thus $pCO_{2(aq,bio)}$. Globally, this biological response in the CSE simulation leads to a decrease in the $pCO_{2(aq,bio)}$ drawdown (-1.4 μatm year^{-1} averaged over $2091-2100$, Fig. 5) and, hence,

https://doi.org/10.5194/egusphere-2025-1495
Preprint. Discussion started: 14 April 2025

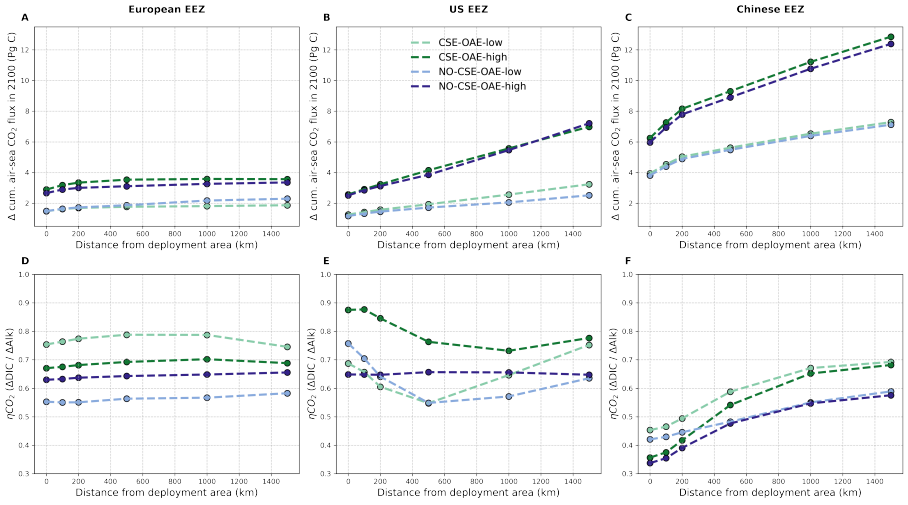

Figure 4. (A, B, C) Cumulative excess ocean CO_2 uptake in 2100 within the deployment regions (0 km distance) and including vicinities of increasing distance (100−1500 km). (D, E, F) The same for the efficiency ηCO_2. Locations and sizes of the vicinity areas are displayed in Fig. A3.

to a weaker ocean CO_2 sink. Secondly, however, the different carbonate system state leads to a slightly larger biological pCO_2 drawdown (+0.1 μatm year^{-1} averaged over 2091−2100, Fig. 5). Note that both effects on the global biological pCO_2 drawdown are not significant. Thus, the stronger global ocean CO_2 sink in the CSE simulations must be fully driven by the state of the carbonate system, facilitated by a lower alkalinity-to-DIC ratio (1.118 in the CSE versus 1.123 in the NO-CSE simulation), a resulting lower buffer capacity and a resulting larger efficiency of OAE (Hinrichs et al., 2023), and not by biological feedbacks. Consistent with the findings in Hinrichs et al. (2023), we find that the baseline alkalinity and DIC concentrations are pivotal for the surface ocean pCO_2 reduction after alkalinity addition, which highlights the need for a careful assessment of the initial carbonate system states in OAE model studies. However, we observe that carbonate system effects on phytoplankton can indeed locally enhance the ocean CO_2 uptake following OAE, for example in the Chinese EEZ where the biological pCO_2 drawdown is significantly increased by +1.0 μatm year^{-1} (Fig. 5).

3.2 OAE effects on biology

In the deployment regions of the simulations with carbonate system effects on phytoplankton, net primary production (NPP) is lower with OAE relative to simulations without OAE, with a significant difference especially in the Chinese EEZ (up to −15% in 2091−2100, Table A4). NPP anomalies globally as well as in the simulations without carbonate system effects (here caused by indirect effects of OAE through radiative feedbacks) are less pronounced (Table A4). In accordance with this, annual NPP anomalies are negatively correlated with surface alkalinity anomalies in the simulations with carbonate system effects on phytoplankton ($p<0.05$, Fig. 6A) but not those without ($p>0.05$, Fig. 6B).

https://doi.org/10.5194/egusphere-2025-1495
Preprint. Discussion started: 14 April 2025

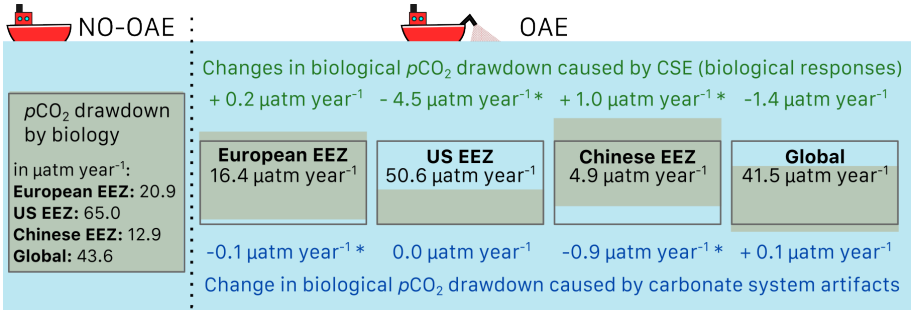

Figure 5. Schematic figure of the biological pCO_2 drawdown summarizing the results presented in Table A3. The size of the boxes represents the weaker biological pCO_2 drawdown resulting from OAE. Modifications of the biological pCO_2 drawdown by carbonate system effects on phytoplankton (green) and by the state of the carbonate system (blue) are represented by changes in the height of the boxes for each deployment region and globally. Positive numbers are an increase in the biological pCO_2 drawdown, negative numbers a decrease. Stars indicate significant changes. Note that the schematics scale only qualitatively, not quantitatively.

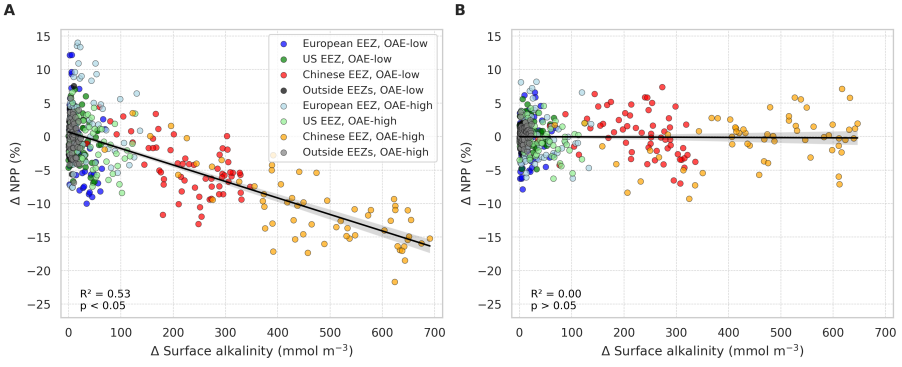

Figure 6. Anomalies of net primary production (NPP) in response to OAE in (A) with carbonate system effects on phytoplankton (CSE-OAE − CSE-NO-OAE) and (B) without carbonate system effects (NO-CSE-OAE − NO-CSE-NO-OAE) simulations, respectively, plotted against anomalies in surface alkalinity. NPP and surface alkalinity anomalies were plotted separately for each year and deployment region. Regression lines, R^2, and p-values were computed together for all datapoints in one panel. Grey shadings represent the 95% confidence interval of the fitted lines.

Decreasing NPP in the CSE-OAE simulations within the deployment areas is mainly driven by diatoms (significant negative correlation of diatom NPP with amount of alkalinity added, Fig. 7A) and slightly dampened by small phytoplankton (significant positive correlation of small phytoplankton NPP and amount of alkalinity added, Fig. 7B). Enhanced small phytoplankton NPP cannot fully balance the lower diatom NPP because of its smaller contribution to overall NPP (e.g., 3% small phytoplankton versus 97% diatoms in the Chinese EEZ, 40% versus 58% in the US EEZ). Nevertheless, within the bounds of the phytoplankton community described in our model, this indicates a community shift towards fewer large cells (diatoms) and more small cells (small phytoplankton) assuming unchanged grazing pressure on each group. Modifications in small phytoplankton and

https://doi.org/10.5194/egusphere-2025-1495
Preprint. Discussion started: 14 April 2025

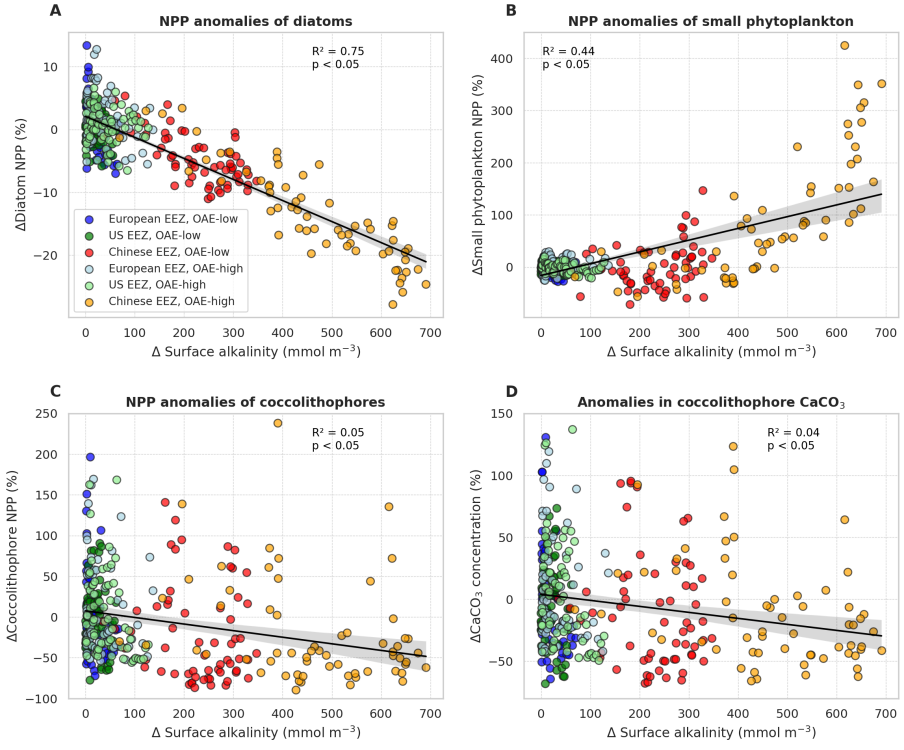

Figure 7. Anomalies of net primary production (NPP) and concentrations of calcium carbonate ($CaCO_3$) in response to OAE (CSE-OAE − CSE-NO-OAE) plotted against anomalies in surface alkalinity. (A) Diatom NPP, (B) small phytoplankton NPP, (C) coccolithophore NPP, and (D) $CaCO_3$ produced by coccolithophores. NPP, $CaCO_3$, and surface alkalinity anomalies were plotted separately for each year and deployment region. Regression lines, R^2, and p-values were computed together for all datapoints in one panel. Grey shadings represent the 95% confidence interval of the fitted lines.

diatom NPP in the NO-CSE-OAE simulations are not correlated with the amount of added alkalinity (Fig. A5A,B).

Both coccolithophore NPP and $CaCO_3$ of the CSE-OAE simulations decrease significantly with increasing alkalinity addition inside the deployment regions (Fig. 7C,D, Table A5). In the simulation without carbonate system effects, where calcification is performed by a fixed share of small phytoplankton, changes in $CaCO_3$ and the amount of added alkalinity are not correlated (Fig. A5C, Table A5). While the PIC:POC ratio in the NO-CSE simulations is defined to be constant, both coccolithophore PIC and POC can vary independently from each other in the CSE simulations. A significantly higher PIC:POC ratio in the European EEZ and globally in the OAE-high simulation with carbonate system effects on phytoplankton (+0.01, resulting in PIC:POC ratios of 1.18 and 1.14, respectively, Table A5) points towards more strongly calcifying coccolithophores, while a decreasing PIC:POC ratio in the Chinese EEZ (-0.05, resulting in a ratio of 1.10, Table A5) reflects lighter calcifying

https://doi.org/10.5194/egusphere-2025-1495
Preprint. Discussion started: 14 April 2025

coccolithophores.

To assess whether the CO_2 factor is the primary driver of the negative correlation between OAE and NPP as well as $CaCO_3$ concentration, we examined changes in the factor over the time period of the OAE deployment. In some years before 2070, the CO_2 factor is smaller in the OAE compared to the NO-OAE simulations in the European and the US EEZ because of the small OAE signal caused by low alkalinity additions (Fig. 8A,B,D,E). At the latest from 2070 onwards, the factor is always higher in the CSE-OAE simulations relative to the CSE-NO-OAE simulations (Fig. 8). Hence, OAE is always beneficial for gross photosynthesis and calcification within the assumptions of our model, rejecting the hypothesis of strengthened CO_2 limitation due to OAE.

Instead, the inverse response of small phytoplankton and diatoms to OAE is likely caused by a stronger increase in the CO_2 factor of small phytoplankton (Fig. 8A,B,C). Indeed, our parameter choice in $f(CO_2)_i$ allows for a higher CO_2 factor for small phytoplankton in comparison to diatoms under increasing alkalinity concentrations (Fig. 1A), pointing towards a competitive advantage of small phytoplankton over diatoms. It was shown in Seifert et al. (2022) that small modifications in the CO_2 factors can trigger considerable shifts in the phytoplankton community, even by a phytoplankton group that is less represented in the respective region. Hence, the unequal increase rather than a decrease in the CO_2 factor are the likely causes for decreasing diatom and increasing small phytoplankton NPP. Decreasing diatom NPP can be further enhanced by indirect OAE effects that are caused by OAE-induced modifications in the atmospheric CO_2 which changes the radiative balance, winds, and, finally, the mixed layer depth and other drivers that have the potential to modify bottom-up and top-down effects on phytoplankton (similar to Nagwekar et al., 2025).

The stronger increase in the CO_2 factor of calcification relative to coccolithophore NPP (Fig. 8D−F) would suggest that the PIC:POC ratio should increase by 2100. We see this in the European EEZ and globally (Table A5), but not in the other EEZs. Similar to our interpretation of decreasing diatom NPP, we hypothesize that indirect OAE effects as well as the competition with the other phytoplankton groups dominate here, which is supported by the fact that both coccolithophore NPP and $CaCO_3$ concentrations decrease relative to the NO-OAE simulations despite the increasing CO_2 factor. Furthermore, coccolithophore biomass (not NPP) can be modified by changes in the grazing pressure, resulting in changes in the PIC:POC ratio that deviate from modifications in NPP.

3.3 Effects of limited OAE

Our simulations show that OAE can decrease NPP significantly through the coupling of direct OAE responses (i.e., the CO_2 factor) to indirect feedbacks (e.g., competition, cascading effects on bottom-up and top-down drivers). Adding half of the amount of alkalinity (CSE-OAE-low versus CSE-OAE-high) effectively reduces the decline of total NPP in the Chinese EEZ by 60% (3.96 g C m^{-2} $year^{-1}$ versus 9.18 g C m^{-2} $year^{-1}$), but the NPP decline in the European EEZ is four times higher than in the OAE-high simulation (2.48 g C m^{-2} $year^{-1}$ versus 0.61 g C m^{-2} $year^{-1}$, Table A4). Moreover, the reduction in atmo-

https://doi.org/10.5194/egusphere-2025-1495
Preprint. Discussion started: 14 April 2025

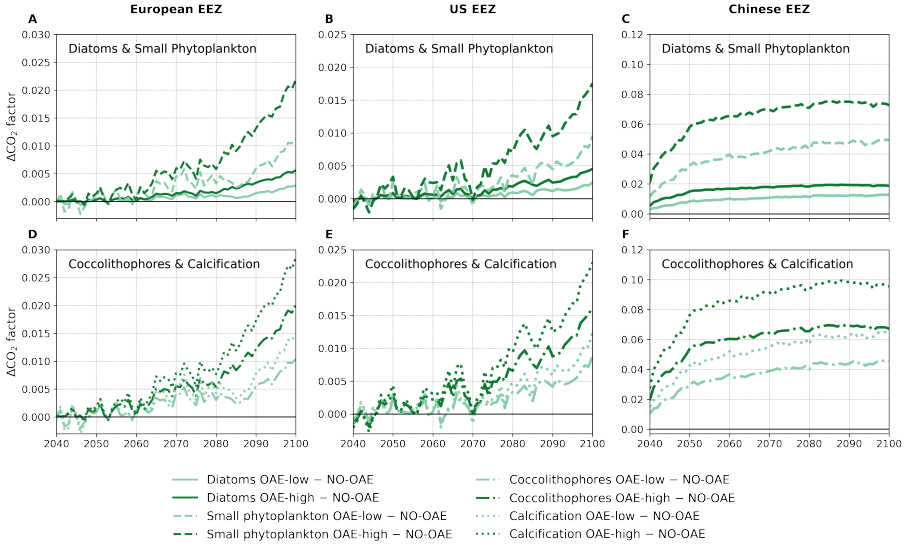

Figure 8. Anomalies of the CO_2 factor in the deployment regions of the CSE-OAE simulations for (A, B, C) diatoms and small phytoplankton, and (D, E, F) coccolithophores and calcification relative to the CSE-NO-OAE simulations. The factor was computed offline from the surface carbonate system using Eq. 3. Note the different y-axes for the three regions.

spheric pCO_2 by 2100 scales with the amount of alkalinity added, reaching only about 50% in the CSE-OAE-low simulation compared to the CSE-OAE-high simulation (2.9 μatm versus 5.7 μatm, Table 1). This poses the question of whether a more targeted limitation of alkalinity addition could mitigate OAE impacts on phytoplankton while preserving CDR effectiveness.

With the motivation to avoid conditions in which abiotic $CaCO_3$ precipitation could happen, we complemented a CSE-OAE-high simulation in which no alkalinity was added to a grid cell when the saturation state of aragonite exceeded 10 (CSE-OAE-high-lim). Only the Chinese EEZ is affected by limited alkalinity addition by adding up to 4 mol alkalinity m^{-2} $year^{-1}$ (about 10%) less than in the CSE-OAE-high simulation, resulting in increasing surface alkalinity by 469 mmol m^{-3} instead of 649 mmol m^{-3}. The significant NPP decrease in the Chinese EEZ of the CSE-OAE-high-lim simulation is dampened to 48% of the CSE-OAE-high simulation (4.75 g C m^{-2} $year^{-1}$ versus 9.18 g C m^{-2} $year^{-1}$), similar to the CSE-OAE-low simulation. The significant NPP decline in CSE-OAE-high-lim in the European EEZ is still stronger than in the CSE-OAE-high simulation (2.01 g C m^{-2} $year^{-1}$ versus 0.61 g C m^{-2} $year^{-1}$), but less strong than in the CSE-OAE-low simulation (2.48 g C m^{-2} $year^{-1}$, Table A4). NPP in the US EEZ decreases, however, more (up to 37%) than in both, CSE-OAE-low and CSE-OAE-high. The decrease of the PIC:POC ratio in the Chinese EEZ vanishes, while PIC:POC anomalies in the other EEZs and globally are comparable to the CSE-OAE-high simulation (Table A5). Whereas the OAE effects on the ecosystem with limited alkalinity addition are often smaller compared to the CSE-OAE-high simulation, it even increases the CDR effectiveness: atmospheric pCO_2 in the CSE-OAE-high-lim simulation is reduced by 7% more (6.1 μatm) than in the CSE-OAE-high simulation (5.7 μatm, Table 1).

https://doi.org/10.5194/egusphere-2025-1495
Preprint. Discussion started: 14 April 2025

4 Discussion

Marine CDR approaches are often less well perceived by the public than terrestrial methods (Cox et al., 2021). This is explicitly true for approaches in which material is released, such as OAE (Bertram and Merk, 2020), highlighting the need to develop a robust understanding of the risks and uncertainties of OAE. Our study aims to shed light on the large-scale interaction between OAE and the marine ecosystem.

4.1 Half of the excess CO_2 uptake occurs outside the deployment regions

With up to 1 Pg C year^{-1} (in the CSE-OAE-high simulation, with a global alkalinity input of 96 Tmol year^{-1}), OAE has the potential to sequester more than seven times as much atmospheric CO_2 in the ocean than natural rock weathering (0.14 Pg C year^{-1}, Renforth and Henderson, 2017) and about 40−60% of the residual and hard-to-abate emissions (1.6−2.7 Pg C year^{-1}, Smith et al., 2024). Approximately 50% of this excess CO_2 flux occurs outside the deployment regions, partly even in the periphery of 1500 km, likely depending on the prevailing surface ocean currents in the deployment region that transport the alkaline material away from its initial injection site. A similar share was observed in the coastal OAE model study of Palmiéri and Yool (2024). These dynamics will complicate "Monitoring, reporting, and verification" (MRV) processes (quantify the effectiveness of CDR activities) as they require to track patches of artificially elevated alkalinity beyond the deployment region to fully assess the excess CO_2 taken up by the ocean (Ho et al., 2023). Further complicating MRV, our study shows that the enhanced ocean sink by OAE is in parts compensated, or even overcompensated, by a reduced land sink, in line with previous studies (e.g., Palmiéri and Yool, 2024; Jeltsch-Thömmes et al., 2024). This leads to a smaller reduction in atmospheric pCO_2 than would be expected from monitoring the air-sea CO_2 flux alone (this study, Schwinger et al., 2024).

4.2 Biological feedbacks modify the strength of ocean CO_2 uptake via OAE

Globally, carbonate system effects on phytoplankton are not the reason for higher air-sea CO_2 fluxes in the CSE compared to the NO-CSE simulation, but rather dissimilarities in initial surface alkalinity and DIC caused by differences in representations of the $CaCO_3$ cycle in the two model versions. In the European and Chinese EEZ, however, we indeed see that carbonate system effects on phytoplankton increase the potential of the ocean to take up atmospheric CO_2 relative to the NO-CSE simulations. This has implications for MRV as it suggests that biological feedbacks need to be taken into account when assessing the excess ocean CO_2 sink resulting from OAE.

4.3 Indirect OAE effects lead to decreasing NPP

We found that OAE-induced anomalies in surface alkalinity correlate with a decrease in total NPP. As the CO_2 factor, the primary link between changes in the carbonate system and phytoplankton photosynthesis, does not imply reduced growth, other indirect OAE effects must diminish NPP. In fact, this is in line with the hypothesis of Bach et al. (2019) that shifts in the carbonate system by OAE are too small to trigger a significant effect on productivity. An imbalance in the change of the CO_2 factor between phytoplankton groups can, yet, result in a modified habitat competition in bottom-up and top-down fac-

https://doi.org/10.5194/egusphere-2025-1495
Preprint. Discussion started: 14 April 2025

tors at the expense of the dominant phytoplankton group. A similar finding for the CO_2 factor, termed as "cascading effects", was described by Seifert et al. (2022). Positive or neutral OAE effects on phytoplankton in laboratory studies must, thus, not necessarily result in positive or no effects of OAE on primary producers in the real ocean. Point-observations of the plankton community before, during, and after OAE applications would increase the understanding of direct and indirect ecosystem responses to OAE.

Our simulations do not confirm the beneficial effect of OAE on coccolithophores which was hypothesized by Bach et al. (2019). NPP of coccolithophores decreases with progressing OAE, and PIC:POC only increases in the Chinese EEZ - both increasing coccolithophore NPP and PIC:POC ratios would have been a sign of the "white ocean" (Bach et al., 2019). Accordingly, our study could not confirm the reduction of surface alkalinity by enhanced calcification which would reduce the efficiency of OAE (part of the "leakage term", Ho et al., 2023). It has to be noted, however, that our alkalinity addition is only up to 10% of the addition required to trigger coccolithophore proliferation according to Lehmann and Bach (2025) (1.1 Pmol year^{-1} versus a total of 0.1 Pmol year^{-1} in 2100 in our simulations). Furthermore, coccolithophores constitute only a very small part ($<0.1-0.8\%$) of the phytoplankton community in the deployment regions of our model. In the real ocean, however, the deployment regions do host coccolithophore blooms (Daniels et al., 2018). Repeating the simulations with OAE deployment in coccolithophore hotspots of our model (e.g., the North Atlantic and the Equatorial Pacific) instead of the EEZs or improving the coastal coccolithophore representation in our model could provide further insights into the alkalinity leakage.

4.4 Maximizing efficiency and minimizing environmental impacts requires delicate selection of OAE amount and location

Deploying only half of the alkalinity reduces the effects on the ecosystem, but comes along with only 50% atmospheric pCO_2 reduction. Reducing the OAE deployment more locally (in this study, the reduction depends on the saturation state of aragonite) can be as or even more effective than deploying as much alkalinity as possible, while minimizing the effects on the ecosystem. Hence, in future OAE applications it is about finding the optimum between effectiveness and environmental impact. This optimum is likely unique for each deployment region, which hinders us to give quantitative suggestions for the ideal amount of alkalinity addition.

4.5 Limitations of the study

The CO_2 factor $f(CO_2)_i$ was initially developed for the description of ocean acidification effects on phytoplankton (Bach et al., 2015; Seifert et al., 2022). Due to the lack of comprehensive data from laboratory experiments, we assumed that the factor likewise works for alkalinity-induced changes in the carbonate system. The laboratory study of Hoppe et al. (2011) is supporting this by showing that pCO_2 manipulations both by alkalinity and by DIC modifications have similar effects on coccolithophore growth rates. Nonetheless, functions tailored for alkalinity enhancement would allow for a more accurate assessment including effects of carbonate system changes on elemental ratios (e.g., Burkhardt et al., 1999; Ferderer et al., 2022; Bhaumik et al.,

https://doi.org/10.5194/egusphere-2025-1495
Preprint. Discussion started: 14 April 2025

2025).

We only consider alkalinity effects on phytoplankton, but zooplankton may be equally sensitive to OAE. Although the study of Sánchez et al. (2024) reveals that the plankton food-web in a mesocosm experiment was relatively resistant to OAE, the authors list potential vulnerabilities that may appear in other plankton communities. For example, zooplankton could be affected by OAE-induced changes in the nutritional value of their prey (Ferderer et al., 2022; Subhas et al., 2022; Bhaumik et al., 2025). Studying community-level effects of OAE in ecosystem models would reveal a better understanding of its large-scale ecosystem effects, but is currently impeded by lacking data on zooplankton-OAE interactions for model parameterizations.

Ensemble simulations would help to quantify the effects of internal variability, thereby giving a better idea of the potential indirect effects of OAE on the ecosystem. However, since our study focuses on direct OAE effects in the upper ocean where the signal-to-noise ratio is high, we consider our study as a robust first step towards a better understanding of the mechanistic effects of OAE on phytoplankton.

5 Conclusions

Our results highlight the need to consider OAE-ecosystem feedbacks when investigating the effectiveness and the environmental impact of OAE. While experimental and mesocosm studies on OAE effects are increasing, little of these findings is used by the modelling community so far. Closer collaborations between both research fields can enhance the understanding of real-world OAE applications, and ultimately help to find a balance between environmental safety and OAE as a necessary CO_2 removal technique to reduce climate change impacts. Future studies should focus on improving the link between OAE and ecosystem by more tailored parameterizations.

Code and data availability. During the revision process, model data is available on figshare via a private link (Seifert et al., 2025). The data will be published with a doi link once the paper has been accepted. The REcoM code is the same as in Seifert et al. (2022) and available online (Seifert and Hauck, 2022).

Appendix A: Description of REcoM

Our ocean biogeochemistry model REcoM is characterized by representing the ecosystem with variable intracellular stoichiometric ratios (carbon : nitrogen : chlorophyll for phytoplankton, Schartau et al., 2007; Hauck et al., 2013) which allow a flexible adaptation to prevailing environmental conditions following the photoacclimation model of Geider et al. (1998). The phytoplankton functional group of diatoms additionally incorporates a flexible stoichiometry for silicic acid, with varying degree of silicification through the decoupling between nutrient uptake and silicification (Claquin et al., 2002; Hohn, 2009). Intracellular iron concentrations are derived from a fixed iron : nitrogen ratio. While the classification of diatoms is taxonomic, the small

https://doi.org/10.5194/egusphere-2025-1495
Preprint. Discussion started: 14 April 2025

phytoplankton comprises a wide range of taxa, such as non-silicifying and non-calcifying haptophytes and green algae.

Zooplankton intracellular stoichiometry is defined by carbon and nitrogen. The generic zooplankton group is distributed globally, while the polar macrozooplankton is restricted to the Southern Ocean and the northern high latitudes (Karakuş et al., 2021). Grazing is described by a sigmoidal function of variable preference (Fasham et al., 1990), with relatively higher grazing rates and a higher preference for small phytoplankton of the generic zooplankton, and relatively lower grazing rates and a higher preference for diatoms of the polar macrozooplankton (Seifert et al., 2022).

Sources for the slow-sinking detritus group are phytoplankton aggregation as well as sloppy feeding (which implicitly included defecation of the generic zooplankton group) and mortality of zooplankton. Fast-sinking detritus is only increased by sloppy feeding, mortality, and fecal pellet production of the polar macrozooplankton group. Detritus carbon and nitrogen is reduced by zooplankton grazing and the degradation to dissolved organic matter (Hauck et al., 2013; Karakuş et al., 2021). The sinking speed of the slow-sinking detritus groups is 20 m day^{-1} at the surface and increases linearly with depth Hauck et al. (2013). The sinking speed of the fast-sinking detritus group is with 200 m day^{-1} constant throughout the water column. Sinking material that reaches the seafloor (single-layer sediment pool in REcoM) is subsequently released back to the lowermost depth layer of the water column.

Appendix B: Description of the phytoplankton gross photosynthesis in REcoM

Gross photosynthesis in REcoM of phytoplankton group i is dependent on temperature ($f(T)_i$), PAR ($f(PAR)_i$), the availability of nutrients ($f(\mathrm{N})_i$), and − in the CSE simulations − the carbonate system ($f(\mathrm{CO_2})_i$):

$$PS_i = f(T)_i \cdot f(PAR)_i \cdot f(\mathrm{N})_i \cdot f(\mathrm{CO_2})_i. \tag{B1}$$

The temperature dependence of diatom and small phytoplankton follows an Arrhenius equation:

$$f(T)_i = \mathrm{PS}_{max,i} \cdot \exp\left(-4500 \cdot \left[\frac{1}{\mathrm{T}_K} - \frac{1}{\mathrm{T}_{K,ref}}\right]\right), \tag{B2}$$

with T_K being the temperature in the water column in Kelvin, and $\mathrm{T}_{K,ref}$ being the reference temperature of 288.15 K (15°C). $\mathrm{PS}_{max,i}$ describes the group-specific maximum growth rate under non-limiting conditions at 15°C and is set to 3.5 d^{-1} for diatoms and 3.0 d^{-1} for small phytoplankton. For coccolithophores (denoted by a *j*), a different temperature dependence is used based on findings from experimental relations between coccolithophore growth rates and temperature (Fielding, 2013):

$$f(T)_j = \mathrm{PS}_{max,j} \cdot 0.1419 \cdot \mathrm{T}_{\circ C}^{0.8151}, \tag{B3}$$

with $\mathrm{T}_{\circ C}$ being the temperature in the water column in degree Celsius and $\mathrm{PS}_{max,j}$ the scaling factor (2.8 d^{-1}). To exclude coccolithophore growth in polar regions (see Seifert et al., 2022), the function was set to a small value ($2.33 \cdot 10^{-16}$) for temperatures below 0°C.

https://doi.org/10.5194/egusphere-2025-1495
Preprint. Discussion started: 14 April 2025

The dependence of gross photosynthesis on nutrient availability, $f(N)_i$, is determined by the most limiting nutrient, whereby limitation by DIN (l_i(DIN)) and dissolved silicic acid (l_i(DSi)) depend on the intracellular nitrogen or silicate-to-carbon ratios and the group-specific half-saturation constant for both nutrients (Hauck et al., 2013). Limitation by dissolved iron (l_i(DFe)) is described by a Michaelis-Menten equation that depends on the group-specific half-saturation constant for DFe (for values of half-saturation constants see Seifert et al., 2022). The final nutrient limitation for coccolithophores and small phytoplankton is then described as:

$$f(N)_i = \min(\mathrm{l}_i(\mathrm{DIN}), \mathrm{l}_i(\mathrm{DFe})), \tag{B4}$$

with 0 denoting complete limitation and 1 denoting no limitation. For diatoms, the limitation by DSi (l_i(DSi)) is added within the minimum function.

The effect of PAR on gross photosynthesis, $f(PAR)_i$, follows Geider et al. (1998):

$$f(PAR)_i = 1 - \exp\left(\frac{-\alpha_j \cdot \mathrm{q}_j^{Chl:C} \cdot PAR}{f(T)_i \cdot f(N)_i}\right). \tag{B5}$$

In addition to the available PAR in the water column it depends on the group-specific maximum light harvesting efficiency α_j (for numbers see Seifert et al., 2022), the variable chlorophyll-to-carbon ratio $\mathrm{q}_j^{Chl:C}$, and the dependence of gross photosynthesis on temperature and nutrient availability, allowing for flexible adaptation to the prevailing light conditions depending on the available resources and temperature. The last term in the function of gross photosynthesis, $f(CO_2)_i$, is described in detail in the main text.

Appendix C: Description of calcification in REcoM

Calcification follows the description in Seifert et al. (2022), which builds on the model functions defined in Krumhardt et al. (2017). The temperature dependence of coccolithophore calcification (denoted by a *j*), $f(T)_{j,calc}$, is described as:

$$f(T)_{j,calc} = \begin{cases} 0.104 \cdot \mathrm{T}_{\circ\mathrm{C}} - 0.108 & \text{if } \mathrm{T}_{\circ\mathrm{C}} < 10.6°C \\ 1 & \text{if } \mathrm{T}_{\circ\mathrm{C}} \geq 10.6°C \end{cases} \tag{C1}$$

where $\mathrm{T}_{\circ_C}$ describes the temperature in degree Celsius. The nutrient dependence of calcification was originally described as a dependence on phosphate limitation in Krumhardt et al. (2017), and translated to DIN limitation in Seifert et al. (2022) as REcoM does not describe the cycling of phosphate. Hence, $f(N)_{j,calc}$ is described as:

$$f(N)_{j,calc} = \mathrm{x} \cdot \left(\frac{[\mathrm{DIN}]}{[\mathrm{DIN}] \cdot \mathrm{k}_{j,DIN}} + \mathrm{y}\right), \tag{C2}$$

with [DIN] being the concentration of dissolved inorganic nitrogen in the water column and $\mathrm{k}_{j,DIN}$ being the half-saturation constant for nitrate uptake of coccolithophores. We use x = -0.31 and y = 1.31 to describe the increase of the PIC:POC ratio by 25% under nitrate-limited compared to nitrate-repleted conditions (Seifert et al., 2022).

https://doi.org/10.5194/egusphere-2025-1495
Preprint. Discussion started: 14 April 2025

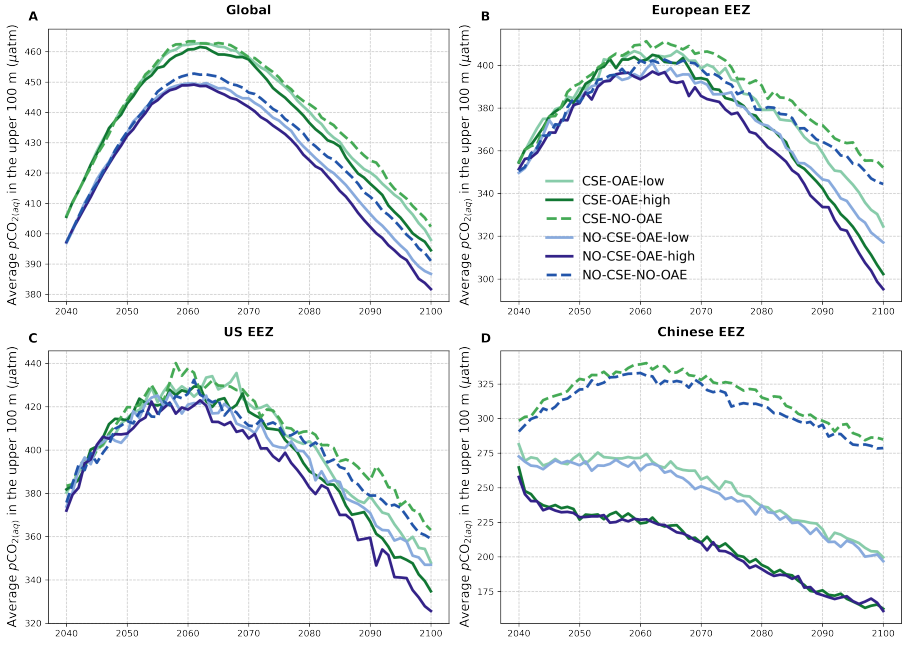

Figure A1. Time series of average $pCO_{2(aq)}$ in the upper 100 m of the watercolumn (A) globally and in the (B) European, (C) US, and (D) Chinese EEZ from the start of the alkalinity enhancement (2040) to the end of the century (2100).

https://doi.org/10.5194/egusphere-2025-1495
Preprint. Discussion started: 14 April 2025

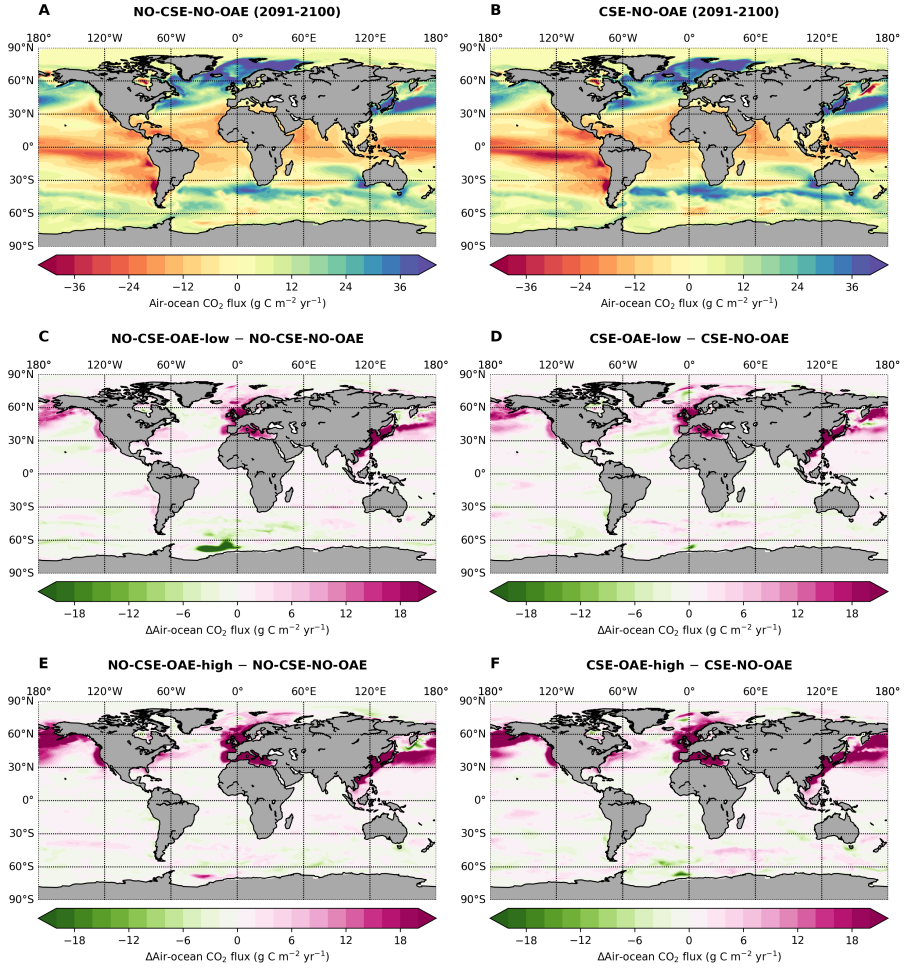

Figure A2. Air-sea CO_2 flux, mean of 2091−2100 (A, C, E) in the NO-CSE simulations, and (B, D, F) in the CSE simulations. Positive numbers in (A) and (B): ocean sink, negative numbers: ocean source. Fluxes in (C−F) are displayed as anomalies relative to the NO-OAE simulations; (C, D) for the OAE-low simulations, and (E, F) for the OAE-high simulations.

https://doi.org/10.5194/egusphere-2025-1495
Preprint. Discussion started: 14 April 2025

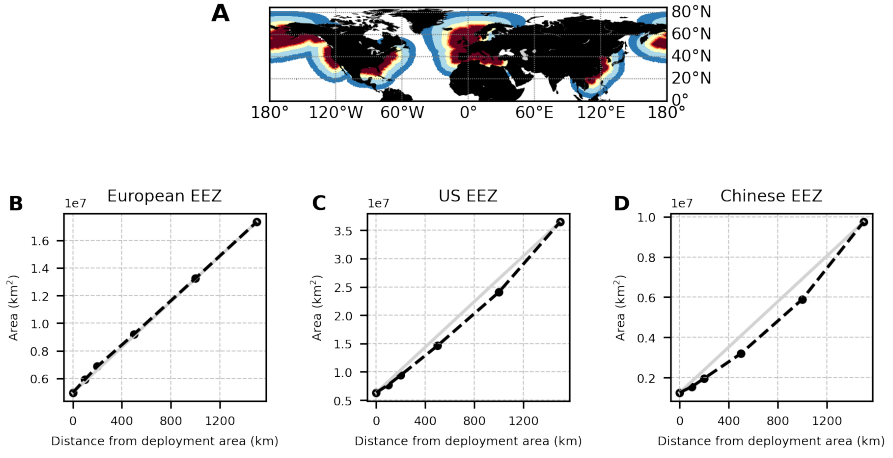

Figure A3. (A) Vicinities included in the computation of air-sea CO_2 fluxes and efficiencies in addition to the deployment regions (dark red): +100 km(lighter red), +200 km (orange), +500 km (yellow), +1000 km (light blue), +1500 km (dark blue). (B, C, D) Total area of the additional vicinities in the three deployment regions. Light grey lines indicate a linear increase from the area of the deployment regions to the area of the largest vicinity (+1500 km) for reference.

https://doi.org/10.5194/egusphere-2025-1495
Preprint. Discussion started: 14 April 2025

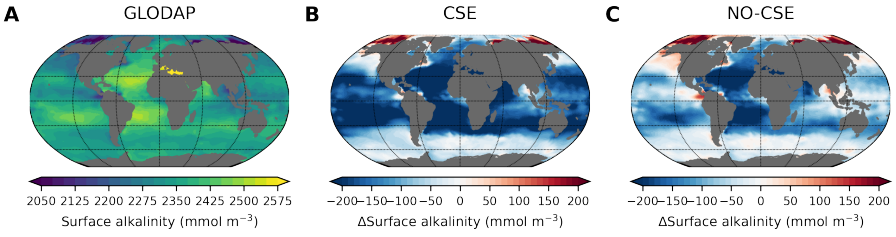

Figure A4. Anomalies in model surface ocean alkalinity compared to observations. (A) Surface ocean alkalinity in the gridded data product GLODAPv2 (data from 1971−2013; Lauvset et al., 2016). (B, C) Present-day surface alkalinity (mean 2010−2014 of the historical simulations) in the CSE and the NO-CSE simulation.

https://doi.org/10.5194/egusphere-2025-1495
Preprint. Discussion started: 14 April 2025

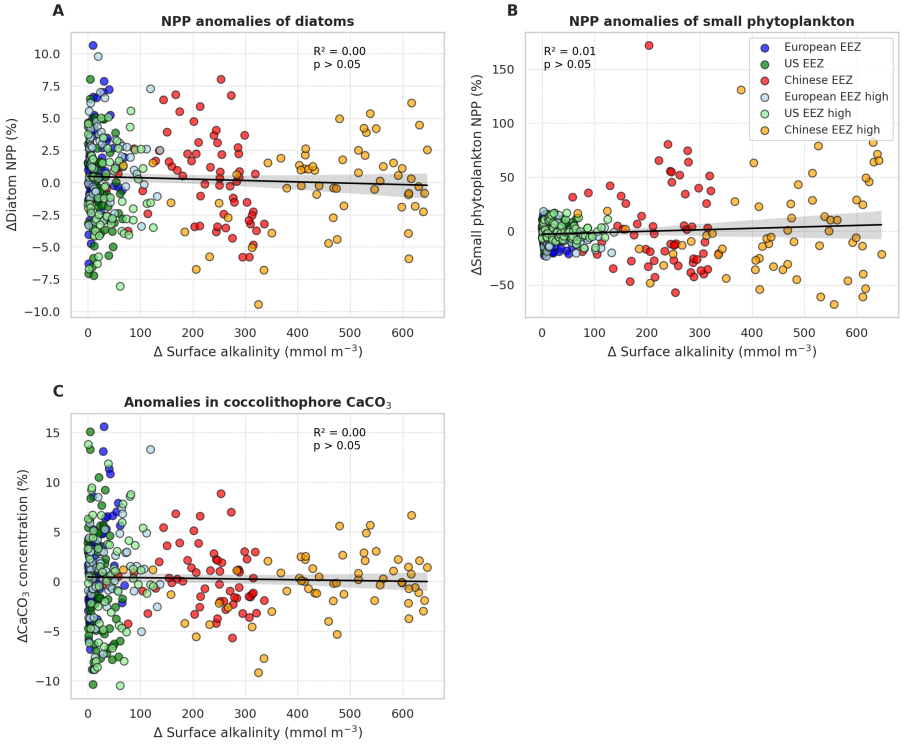

Figure A5. Anomalies of net primary production (NPP) and concentrations of calcium carbonate ($CaCO_3$) in the NO-CSE-OAE simulations relative to the NO-CSE-NO-OAE simulations plotted against anomalies in surface alkalinity. (A) Diatom NPP, (B) small phytoplankton NPP, and (C) $CaCO_3$ produced by a fixed share (2%) of small phytoplankton. NPP, $CaCO_3$, and surface alkalinity anomalies were plotted separately for each year and deployment region. Regression lines, R^2, and p-values were computed together for all datapoints in one panel. Grey shadings represent the 95% confidence interval of the fitted lines.

https://doi.org/10.5194/egusphere-2025-1495
Preprint. Discussion started: 14 April 2025

Table A1. Parameters for the CO_2 factor (Equation 3) following Seifert et al. (2022). PS = gross photosynthesis.

Process	a (dimensionless)	b (mol kg^{-1})	c (kg mol^{-1})	d (kg mol^{-1})
Diatom PS	1.040	28.90	0.8778	$2.640 \cdot 10^6$
Small phytoplankton PS	1.162	48.88	0.255	$1.023 \cdot 10^7$
Coccolithophore PS	1.109	37.67	0.3912	$9.450 \cdot 10^6$
Calcification	1.102	42.38	0.7079	$1.343 \cdot 10^7$

https://doi.org/10.5194/egusphere-2025-1495
Preprint. Discussion started: 14 April 2025

Table A2. Relative contribution to anomalies in air-sea CO_2 fluxes and OAE efficiencies within the deployment regions and the 1000 km vicinity (vic.). "Rest": global minus deployment regions; "Global": including deployment regions.

	Relative contribution to anomalies in air-sea CO_2 flux (%), 2100				OAE efficiency (ΔDIC / ΔAlkalinity), mean 2091−2100			
	Europe + vic.	USA + vic.	China + vic.	Rest	Europe + vic.	USA + vic.	China + vic.	Global
CSE-OAE-low	14.3	20.6	51.7	13.8	0.79	0.65	0.67	0.72
CSE-OAE-high	13.8	21.4	43.1	21.7	0.70	0.73	0.65	0.73
NO-CSE-OAE-low	19.1	18.0	56.1	6.8	0.57	0.57	0.55	0.66
NO-CSE-OAE-high	14.6	24.4	48.1	12.9	0.65	0.66	0.55	0.62

https://doi.org/10.5194/egusphere-2025-1495
Preprint. Discussion started: 14 April 2025

Table A3. Annual sum of the surface ocean biological pCO_2 drawdown averaged over 2091-2100. Positive signs denote biological pCO_2 drawdown, negative signs denote a counteractive effect on biological pCO_2 drawdown. Diff = OAE-high minus NO-OAE.

Biological pCO_2 drawdown in the upper 100 m...	Computation	Europe (μatm year^{-1})			USA (μatm year^{-1})			China (μatm year^{-1})			Global (μatm year^{-1})		
		OAE-high	NO-OAE	Diff	OAE-high	NO-OAE	Diff	OAE-high	NO-OAE	Diff	OAE-high	NO-OAE	Diff
... with CO_2 effects on phytoplankton and carbonate system changes	$\frac{\Delta \mathrm{DIC}_{bio,CSE}}{\gamma \mathrm{DIC}_{CSE}} \cdot pCO_{2(aq),CSE}$	+16.4	+20.9	-4.5	+50.6	+65.0	-14.4	+4.9	+12.9	-8.0	+41.5	+43.6	-2.1
... with CO_2 effects on phytoplankton and no carbonate system changes	$\frac{\Delta \mathrm{DIC}_{bio,CSE}}{\gamma \mathrm{DIC}_{NO-CSE}} \cdot pCO_{2(aq),NO-CSE}$	+15.7	+20.1	-4.4	+47.6	+62.0	-14.4	+4.8	+11.9	-7.1	+38.6	+40.8	-2.2
... with carbonate system changes but no CO_2 effects on phytoplankton	$\frac{\Delta \mathrm{DIC}_{bio,NO-CSE}}{\gamma \mathrm{DIC}_{CSE}} \cdot pCO_{2(aq),CSE}$	+19.9	+24.6	-4.7	+55.1	+65.0	-9.9	+6.7	+15.7	-9.0	+41.0	+41.7	-0.7
Carbonate system effects	row 1 — row 2	+0.7	+0.8	**-0.1**	+3.0	+3.0	**0.0**	+0.1	+1.0	**-0.9**	+2.9	+2.8	**+0.1**
Biological effects	row 1 — row 3	-3.5	-3.7	**+0.2**	-4.5	0.0	**-4.5**	-1.8	-2.8	**+1.0**	+0.5	+1.9	**-1.4**

https://doi.org/10.5194/egusphere-2025-1495
Preprint. Discussion started: 14 April 2025

Table A4. Anomalies in net primary production (NPP) in the OAE simulations relative to the NO-OAE simulations, averaged over 2091-2100. Stars indicate significant difference to the respective NO-OAE simulation.

	Total NPP anomalies ($g\,C\,m^{-2}\,year^{-1}$), mean 2091−2100				Relative NPP anomalies (%), mean 2091−2100			
	Europe	USA	China	Global	Europe	USA	China	Global
CSE-OAE-low	-2.48*	-2.24	-3.96*	+0.10	-4.2*	-2.2	-6.4*	+0.2
CSE-OAE-high	-0.61	-2.66*	-9.18*	-0.33	-0.9	-2.6*	-14.7*	-0.4
NO-CSE-OAE-low	-0.14	+0.27	-2.16*	+0.60*	-0.2	+0.3	-3.0*	+0.8*
NO-CSE-OAE-high	-0.38	-0.85	-0.11	+0.44*	-0.6	-0.9	-0.1	+0.6
CSE-OAE-high-lim	*-2.01**	*-3.07**	*-4.75**	*-0.56*	*-3.3**	*-3.1**	*-7.6**	*-0.7*

https://doi.org/10.5194/egusphere-2025-1495
Preprint. Discussion started: 14 April 2025

Table A5. Anomalies in phytoplankton particulate inorganic carbon (PIC) and particulate inorganic to organic carbon ratios (PIC:POC) in the OAE relative to the NO-OAE simulations. Because PIC:POC is set to a fixed ratio of 1 in the NO-CSE simulation, anomalies are denoted to be constant (const.). Stars indicate significant difference to the respective NO-OAE simulation.

	Phytoplankton PIC anomalies (10^{-3} Tg), mean 2091−2100				Phytoplankton PIC:PIC anomalies (mol C : mol C), mean 2091−2100			
	Europe	USA	China	Global	Europe	USA	China	Global
CSE-OAE-low	-34.6*	-79.8*	-0.3*	+105.5	0.00	0.00	-0.01	0.00
CSE-OAE-high	-16.6	-99.9*	-0.4*	-337.0	+0.01*	0.00	-0.05*	+0.01*
NO-CSE-OAE-low	+12.2*	-8.7*	-0.4	+78.5	const.	const.	const.	const.
NO-CSE-OAE-high	+3.6	+4.0	+0.1	+56.4	const.	const.	const.	const.
CSE-OAE-high-lim	*-17.7**	*-94.0**	*0.0*	*-633.2*	*+0.01**	*0.0*	*+0.01*	*+0.01**
	Total phytoplankton PIC (10^{-3} Tg), mean 2091−2100				Phytoplankton PIC:PIC (mol C : mol C), mean 2091−2100			
CSE-NO-OAE	94.7	253.4	1.2	19437.3	1.17	1.06	1.15	1.13
NO-CSE-NO-OAE	226.2	223.5	44.6	16811.9	1.00	1.00	1.00	1.00

https://doi.org/10.5194/egusphere-2025-1495
Preprint. Discussion started: 14 April 2025

Author contributions. JH and CV aquired the funding for the study. MS, CV, and JH conceptualized the study. MS, CD, and JH developed the methodology, and MS and CD performed the model simulations. The data were investigated by MS with contributions from CD, CV, and JH, and visualizations were created by MS. MS prepared the manuscript with contributions from all co-authors.

Competing interests. The authors declare that they have no conflict of interest.

Acknowledgements. This study has received funding from the European Union's Horizon 2020 research and innovation programme under grant agreement No. 869357 (project OceanNETs, Ocean-based Negative Emission Technologies - analyzing the feasibility, risks, and cobenefits of ocean-based negative emission technologies for stabilizing the climate) and from the Initiative and Networking Fund of the Helmholtz Association (Helmholtz Young Investigator Group Marine Carbon and Ecosystem Feedbacks in the Earth System [MarESys], Grant VH-NG-1301). This study reflects only the author's view and the European Commission and their executive agency are not responsible for any use that may be made of the information it contains. The authors thank the colleagues in work package 4 of the OceanNETs project for fruitful and inspiring discussions. A special thank goes to Antti-Ilari Partanen and Tommi Bergman for the development of the OAE deployment mask.

https://doi.org/10.5194/egusphere-2025-1495
Preprint. Discussion started: 14 April 2025

References

Bach, L. T., Riebesell, U., Gutowska, M. A., Federwisch, L., and Schulz, K. G.: A unifying concept of coccolithophore sensitivity to changing carbonate chemistry embedded in an ecological framework, Progress in Oceanography, 135, 125–138, https://doi.org/10.1016/j.pocean.2015.04.012, 2015.

Bach, L. T., Gill, S. J., Rickaby, R. E. M., Gore, S., and Renforth, P.: CO_2 Removal With Enhanced Weathering and Ocean Alkalinity Enhancement: Potential Risks and Co-benefits for Marine Pelagic Ecosystems, Frontiers in Climate, 1, https://doi.org/10.3389/fclim.2019.00007, 2019.

Bednaršek, N., van de Mortel, H., Pelletier, G., García-Reyes, M., Feely, R. A., and Dickson, A. G.: Assessment framework to predict sensitivity of marine calcifiers to ocean alkalinity enhancement – identification of biological thresholds and importance of precautionary principle, Biogeosciences, 22, 473–498, https://doi.org/10.5194/bg-22-473-2025, 2025.

Bertram, C. and Merk, C.: Public Perceptions of Ocean-Based Carbon Dioxide Removal: The Nature-Engineering Divide?, Frontiers in Climate, 2, https://doi.org/10.3389/fclim.2020.594194, 2020.

Bhaumik, A., Faucher, G., Henning, M., Meunier, C. L., and Boersma, M.: Prey dynamics as a buffer: enhancing copepod resilience to ocean alkalinity enhancement, Environmental Research Letters, 20, 024 058, https://doi.org/10.1088/1748-9326/adaa8c, 2025.

Boysen, L. R., Lucht, W., and Gerten, D.: Trade-offs for food production, nature conservation and climate limit the terrestrial carbon dioxide removal potential, Global Change Biology, 23, 4303–4317, https://doi.org/https://doi.org/10.1111/gcb.13745, 2017.

Buck, H. J., Carton, W., Lund, J. F., and Markusson, N.: Why residual emissions matter right now, Nature Climate Change, 13, 351–358, https://doi.org/10.1038/s41558-022-01592-2, 2023.

Burkhardt, S., Zondervan, I., and Riebesell, U.: Effect of CO_2 concentration on C:N:P ratio in marine phytoplankton: A species comparison, Limnology and Oceanography, 44, 683–690, https://doi.org/10.4319/lo.1999.44.3.0683, 1999.

Burns, W. and Corbett, C. R.: Antacids for the Sea? Artificial Ocean Alkalinization and Climate Change, One Earth, 3, 154–156, https://doi.org/https://doi.org/10.1016/j.oneear.2020.07.016, 2020.

Butenschön, M., Lovato, T., Masina, S., Caserini, S., and Grosso, M.: Alkalinization Scenarios in the Mediterranean Sea for Efficient Removal of Atmospheric CO_2 and the Mitigation of Ocean Acidification, Frontiers in Climate, 3, 14, https://doi.org/10.3389/fclim.2021.614537, 2021.

Caserini, S., Storni, N., and Grosso, M.: The Availability of Limestone and Other Raw Materials for Ocean Alkalinity Enhancement, Global Biogeochemical Cycles, 36, e2021GB007 246, https://doi.org/https://doi.org/10.1029/2021GB007246, 2022.

Chrachri, A., Hopkinson, B. M., Flynn, K., Brownlee, C., and Wheeler, G. L.: Dynamic changes in carbonate chemistry in the microenvironment around single marine phytoplankton cells, Nature Communications, 9, 74, https://doi.org/10.1038/s41467-017-02426-y, 2018.

Claquin, P., Martin-Jézéquel, V., Kromkamp, J. C., Veldhuis, M. J. W., and Kraay, G. W.: Uncoupling of silicon compared with carbon and nitrogen metabolisms and the role of the cell cycle in continous cultures of *Thalassiosira pseudonana* (Bacillariophyceae) under light, nitrogen, and phosphorus control, Journal of Phycology, 38, 922–930, https://doi.org/https://doi.org/10.1046/j.1529-8817.2002.t01-1-01220.x, 2002.

Cox, E., Boettcher, M., Spence, E., and Bellamy, R.: Casting a Wider Net on Ocean NETs, Frontiers in Climate, 3, https://doi.org/10.3389/fclim.2021.576294, 2021.

Daniels, C. J., Poulton, A. J., Balch, W. M., Marañón, E., Adey, T., Bowler, B. C., Cermeño, P., Charalampopoulou, A., Crawford, D. W., Drapeau, D., Feng, Y., Fernández, A., Fernández, E., Fragoso, G. M., González, N., Graziano, L. M., Heslop, R., Holligan, P. M., Hopkins,

https://doi.org/10.5194/egusphere-2025-1495
Preprint. Discussion started: 14 April 2025

J., Huete-Ortega, M., Hutchins, D. A., Lam, P. J., Lipsen, M. S., López-Sandoval, D. C., Loucaides, S., Marchetti, A., Mayers, K. M. J., Rees, A. P., Sobrino, C., Tynan, E., and Tyrrell, T.: A global compilation of coccolithophore calcification rates, Earth System Science Data, 10, 1859–1876, https://doi.org/10.5194/essd-10-1859-2018, 2018.

Danilov, S., Kivman, G., and Schröter, J.: A finite-element ocean model: principles and evaluation, Ocean Modelling, 6, 125–150, https://doi.org/https://doi.org/10.1016/S1463-5003(02)00063-X, 2004.

Egleston, E. S., Sabine, C. L., and Morel, F. M. M.: Revelle revisited: Buffer factors that quantify the response of ocean chemistry to changes in DIC and alkalinity, Global Biogeochem. Cycles, 24, https://doi.org/10.1029/2008GB003407, 2010.

Fakhraee, M., Li, Z., Planavsky, N. J., and Reinhard, C. T.: A biogeochemical model of mineral-based ocean alkalinity enhancement: impacts on the biological pump and ocean carbon uptake, Environmental Research Letters, 18, 044 047, https://doi.org/10.1088/1748-9326/acc9d4, 2023.

Fasham, M. J. R., Ducklow, H. W., and McKelvie, S. M.: A nitrogen-based model of plankton dynamics in the oceanic mixed layer, Journal of Marine Research, 48, 591–639, https://doi.org/10.1357/002224090784984678, 1990.

Faucher, G., Haunost, M., Paul, A. J., Tietz, A. U. C., and Riebesell, U.: Growth response of *Emiliania huxleyi* to ocean alkalinity enhancement, Biogeosciences, 22, 405–415, https://doi.org/10.5194/bg-22-405-2025, 2025.

Feng, E. Y., Koeve, W., Keller, D. P., and Oschlies, A.: Model-Based Assessment of the CO_2 Sequestration Potential of Coastal Ocean Alkalinization, Earth's Future, 5, 1252–1266, https://doi.org/https://doi.org/10.1002/2017EF000659, 2017.

Fennel, K., Long, M. C., Algar, C., Carter, B., Keller, D., Laurent, A., Mattern, J. P., Musgrave, R., Oschlies, A., Ostiguy, J., Palter, J. B., and Whitt, D. B.: Modelling considerations for research on ocean alkalinity enhancement (OAE), State of the Planet, 2-oae2023, 9, https://doi.org/10.5194/sp-2-oae2023-9-2023, 2023.

Ferderer, A., Chase, Z., Kennedy, F., Schulz, K. G., and Bach, L. T.: Assessing the influence of ocean alkalinity enhancement on a coastal phytoplankton community, Biogeosciences, 19, 5375–5399, https://doi.org/10.5194/bg-19-5375-2022, 2022.

Fielding, S. R.: *Emiliania huxleyi* specific growth rate dependence on temperature, Limnology and Oceanography, 58, 663–666, https://doi.org/10.4319/lo.2013.58.2.0663, 2013.

Foteinis, S., Andresen, J., Campo, F., Caserini, S., and Renforth, P.: Life cycle assessment of ocean liming for carbon dioxide removal from the atmosphere, Journal of Cleaner Production, 370, 133 309, https://doi.org/https://doi.org/10.1016/j.jclepro.2022.133309, 2022.

Friedlingstein, P., Allen, M., Canadell, J. G., Peters, G. P., and Seneviratne, S. I.: Comment on "The global tree restoration potential", Science, 366, eaay8060, https://doi.org/10.1126/science.aay8060, 2019.

Fuss, S., Canadell, J. G., Peters, G. P., Tavoni, M., Andrew, R. M., Ciais, P., Jackson, R. B., Jones, C. D., Kraxner, F., Nakicenovic, N., et al.: Betting on negative emissions, Nature climate change, 4, 850–853, https://doi.org/10.1038/nclimate2392, 2014.

Gately, J. A., Kim, S. M., Jin, B., Brzezinski, M. A., and Iglesias-Rodriguez, M. D.: Coccolithophores and diatoms resilient to ocean alkalinity enhancement: A glimpse of hope?, Science Advances, 9, eadg6066, https://doi.org/10.1126/sciadv.adg6066, 2023.

Gattuso, J.-P., Williamson, P., Duarte, C. M., and Magnan, A. K.: The Potential for Ocean-Based Climate Action: Negative Emissions Technologies and Beyond, Frontiers in Climate, 2, https://doi.org/10.3389/fclim.2020.575716, 2021.

Geider, R. J., Maclntyre, H. L., and Kana, T. M.: A dynamic regulatory model of phytoplanktonic acclimation to light, nutrients, and temperature, Limnology and Oceanography, 43, 679–694, https://doi.org/10.4319/lo.1998.43.4.0679, 1998.

Giorgetta, M. A., Jungclaus, J., Reick, C. H., Legutke, S., Bader, J., Böttinger, M., Brovkin, V., Crueger, T., Esch, M., Fieg, K., Glushak, K., Gayler, V., Haak, H., Hollweg, H.-D., Ilyina, T., Kinne, S., Kornblueh, L., Matei, D., Mauritsen, T., Mikolajewicz, U., Mueller, W., Notz, D., Pithan, F., Raddatz, T., Rast, S., Redler, R., Roeckner, E., Schmidt, H., Schnur, R., Segschneider, J., Six, K. D., Stockhause, M.,

https://doi.org/10.5194/egusphere-2025-1495
Preprint. Discussion started: 14 April 2025

Timmreck, C., Wegner, J., Widmann, H., Wieners, K.-H., Claussen, M., Marotzke, J., and Stevens, B.: Climate and carbon cycle changes from 1850 to 2100 in MPI-ESM simulations for the Coupled Model Intercomparison Project phase 5, Journal of Advances in Modeling Earth Systems, 5, 572–597, https://doi.org/https://doi.org/10.1002/jame.20038, 2013.

Hartmann, J., Suitner, N., Lim, C., Schneider, J., Marín-Samper, L., Arístegui, J., Renforth, P., Taucher, J., and Riebesell, U.: Stability of alkalinity in ocean alkalinity enhancement (OAE) approaches – consequences for durability of CO_2 storage, Biogeosciences, 20, 781–802, https://doi.org/10.5194/bg-20-781-2023, 2023.

Hauck, J. and Völker, C.: Rising atmospheric CO_2 leads to large impact of biology on Southern Ocean CO_2 uptake via changes of the Revelle factor, Geophysical Research Letters, 42, 1459–1464, https://doi.org/10.1002/2015GL063070, 2015.

Hauck, J., Völker, C., Wang, T., Hoppema, M., Losch, M., and Wolf-Gladrow, D. A.: Seasonally different carbon flux changes in the Southern Ocean in response to the southern annular mode, Global Biogeochemical Cycles, 27, 1236–1245, https://doi.org/10.1002/2013GB004600, 2013.

Hauck, J., Köhler, P., Wolf-Gladrow, D., and Völker, C.: Iron fertilisation and century-scale effects of open ocean dissolution of olivine in a simulated CO_2 removal experiment, Environmental Research Letters, 11, 024 007, https://doi.org/10.1088/1748-9326/11/2/024007, 2016.

Hinrichs, C., Köhler, P., Völker, C., and Hauck, J.: Alkalinity biases in CMIP6 Earth system models and implications for simulated CO_2 drawdown via artificial alkalinity enhancement, Biogeosciences, 20, 3717–3735, https://doi.org/10.5194/bg-20-3717-2023, 2023.

Ho, D.: Carbon dioxide removal is an ineffective time machine, Nature, 616, https://doi.org/https://doi.org/10.1038/d41586-023-00953-x, 2023.

Ho, D. T., Bopp, L., Palter, J. B., Long, M. C., Boyd, P. W., Neukermans, G., and Bach, L. T.: Monitoring, reporting, and verification for ocean alkalinity enhancement, State of the Planet, 2-oae2023, 12, https://doi.org/10.5194/sp-2-oae2023-12-2023, 2023.

Ho, T.-Y., Quigg, A., Finkel, Z. V., Milligan, A. J., Wyman, K., Falkowski, P. G., and Morel, F. M. M.: The elemental composition of some marine phytoplankton, Journal of Phycology, 39, 1145–1159, https://doi.org/10.1111/j.0022-3646.2003.03-090.x, 2003.

Hohn, S.: Coupling and decoupling of biogeochemical cycles in marine ecosystems, PhD thesis, Universität Bremen, http://nbn-resolving.de/urn:nbn:de:gbv:46-diss000112787, 2009.

Hoppe, C. J. M., Langer, G., and Rost, B.: *Emiliania huxleyi* shows identical responses to elevated pCO_2 in TA and DIC manipulations, Journal of Experimental Marine Biology and Ecology, 406, 54–62, https://doi.org/10.1016/j.jembe.2011.06.008, 2011.

Humphreys, M. P., Lewis, E. R., Sharp, J. D., and Pierrot, D.: PyCO2SYS v1.8: marine carbonate system calculations in Python, Geoscientific Model Development, 15, 15–43, https://doi.org/10.5194/gmd-15-15-2022, 2022.

Jeltsch-Thömmes, A., Tran, G., Lienert, S., Keller, D. P., Oschlies, A., and Joos, F.: Earth system responses to carbon dioxide removal as exemplified by ocean alkalinity enhancement: tradeoffs and lags, Environmental Research Letters, 19, 054 054, https://doi.org/10.1088/1748-9326/ad4401, 2024.

Karakuş, O., Völker, C., Iversen, M., Hagen, W., Gladrow, D. W., Fach, B., and Hauck, J.: Modeling the impact of macrozooplankton on carbon export production in the Southern Ocean, Journal of Geophysical Research: Oceans, 126, e2021JC017 315, https://doi.org/10.1029/2021JC017315, 2021.

Köhler, P., Abrams, J. F., Völker, C., Hauck, J., and Wolf-Gladrow, D. A.: Geoengineering impact of open ocean dissolution of olivine on atmospheric CO_2 , surface ocean pH and marine biology, Environmental Research Letters, 8, 014 009, https://doi.org/10.1088/1748-9326/8/1/014009, 2013.

Krumhardt, K. M., Lovenduski, N. S., Iglesias-Rodriguez, M. D., and Kleypas, J. A.: Coccolithophore growth and calcification in a changing ocean, Progress in Oceanography, 159, 276–295, https://doi.org/10.1016/j.pocean.2017.10.007, 2017.

https://doi.org/10.5194/egusphere-2025-1495
Preprint. Discussion started: 14 April 2025

Lauvset, S. K., Key, R. M., Olsen, A., van Heuven, S., Velo, A., Lin, X., Schirnick, C., Kozyr, A., Tanhua, T., Hoppema, M., Jutterström, S., Steinfeldt, R., Jeansson, E., Ishii, M., Perez, F. F., Suzuki, T., and Watelet, S.: A new global interior ocean mapped climatology: the 1° x 1° GLODAP version 2, Earth System Science Data, 8, 325–340, https://doi.org/10.5194/essd-8-325-2016, 2016.

Lehmann, N. and Bach, L. T.: Global carbonate chemistry gradients reveal a negative feedback on ocean alkalinity enhancement, Nature Geoscience, https://doi.org/10.1038/s41561-025-01644-0, 2025.

Moras, C. A., Bach, L. T., Cyronak, T., Joannes-Boyau, R., and Schulz, K. G.: Ocean alkalinity enhancement – avoiding runaway $CaCO_3$ precipitation during quick and hydrated lime dissolution, Biogeosciences, 19, 3537–3557, https://doi.org/10.5194/bg-19-3537-2022, 2022.

Nagwekar, T., Nissen, C., and Hauck, J.: Ocean Alkalinity Enhancement in Deep Water Formation Regions Under Low and High Emission Pathways, Earth's Future, 12, e2023EF004 213, https://doi.org/https://doi.org/10.1029/2023EF004213, 2024.

Nagwekar, T., Danek, C., Seifert, M., and Hauck, J.: Alkalinity Enhancement in the Subduction Regions: Efficiency, Earth System Feedbacks, and Deep Ocean Carbon Sequestration, submitted to: Environmental Research Letter, 2025.

O'Neill, B. C., Tebaldi, C., van Vuuren, D. P., Eyring, V., Friedlingstein, P., Hurtt, G., Knutti, R., Kriegler, E., Lamarque, J.-F., Lowe, J., Meehl, G. A., Moss, R., Riahi, K., and Sanderson, B. M.: The Scenario Model Intercomparison Project (ScenarioMIP) for CMIP6, Geoscientific Model Development, 9, 3461–3482, https://doi.org/10.5194/gmd-9-3461-2016, 2016.

Orr, J. and Epitalon, J.-M.: Improved routines to model the ocean carbonate system: Mocsy 2.0, Biogeosciences, 8, 485–499, https://doi.org/10.5194/gmd-8-485-2015, 2015.

Oschlies, A., Bach, L. T., Rickaby, R. E. M., Satterfield, T., Webb, R., and Gattuso, J.-P.: Climate targets, carbon dioxide removal, and the potential role of ocean alkalinity enhancement, State of the Planet, 2-oae2023, 1, https://doi.org/10.5194/sp-2-oae2023-1-2023, 2023.

Oziel, L., Gürses, O., Torres-Valdés, S., Hoppe, C. J. M., Rost, B., Karakuş, O., Danek, C., Koch, B. P., Nissen, C., Koldunov, N., Wang, Q., Völker, C., Iversen, M., Juhls, B., and Hauck, J.: Climate change and terrigenous inputs decrease the efficiency of the future Arctic Ocean's biological carbon pump, Nature Climate Change, https://doi.org/10.1038/s41558-024-02233-6, 2025.

Palmiéri, J. and Yool, A.: Global-Scale Evaluation of Coastal Ocean Alkalinity Enhancement in a Fully Coupled Earth System Model, Earth's Future, 12, e2023EF004 018, https://doi.org/https://doi.org/10.1029/2023EF004018, 2024.

Paul, A. J., Haunost, M., Goldenberg, S. U., Hartmann, J., Sánchez, N., Schneider, J., Suitner, N., and Riebesell, U.: Ocean alkalinity enhancement in an open ocean ecosystem: Biogeochemical responses and carbon storage durability, EGUsphere, 2024, 1–31, https://doi.org/10.5194/egusphere-2024-417, 2024.

Ramírez, L., Pozzo-Pirotta, L. J., Trebec, A., Manzanares-Vázquez, V., Díez, J. L., Arístegui, J., Riebesell, U., Archer, S. D., and Segovia, M.: Ocean Alkalinity Enhancement (OAE) does not cause cellular stress in a phytoplankton community of the sub-tropical Atlantic Ocean, EGUsphere, 2024, 1–34, https://doi.org/10.5194/egusphere-2024-847, 2024.

Reick, C. H., Gayler, V., Goll, D., Hagemann, S., Heidkamp, M., Nabel, J. E., Raddatz, T., Roeckner, E., Schnur, R., and Wilkenskjeld, S.: JSBACH 3-The land component of the MPI Earth System Model: documentation of version 3.2, 2021.

Renforth, P. and Henderson, G.: Assessing ocean alkalinity for carbon sequestration, Reviews of Geophysics, 55, 636–674, https://doi.org/10.1002/2016RG000533, 2017.

Riebesell, U., Wolf-Gladrow, D. A., and Smetacek, V.: Carbon dioxide limitation of marine phytoplankton growth rates, Nature, 361, 249–251, 1993.

Schartau, M., Engel, A., Schröter, J., Thoms, S., Völker, C., and Wolf-Gladrow, D.: Modelling carbon overconsumption and the formation of extracellular particulate organic carbon, Biogeosciences, 4, 433–454, https://doi.org/10.5194/bg-4-433-2007, 2007.

https://doi.org/10.5194/egusphere-2025-1495
Preprint. Discussion started: 14 April 2025

Schourup-Kristensen, V., Sidorenko, D., Wolf-Gladrow, D. A., and Völker, C.: A skill assessment of the biogeochemical model REcoM2 coupled to the Finite Element Sea Ice–Ocean Model (FESOM 1.3), Geoscientific Model Development, 7, 2769–2802, https://doi.org/10.5194/gmd-7-2769-2014, 2014.

Schulz, K. G., Bach, L. T., and Dickson, A. G.: Seawater carbonate chemistry considerations for ocean alkalinity enhancement research: theory, measurements, and calculations, State of the Planet, 2-oae2023, 2, https://doi.org/10.5194/sp-2-oae2023-2-2023, 2023.

Schwinger, J., Bourgeois, T., and Rickels, W.: On the emission-path dependency of the efficiency of ocean alkalinity enhancement, Environmental Research Letters, 19, 074 067, https://doi.org/10.1088/1748-9326/ad5a27, 2024.

Seifert, M. and Hauck, J.: REcoM code, Zenodo, https://zenodo.org/records/7457987, 2022.

Seifert, M., Nissen, C., Rost, B., and Hauck, J.: Cascading effects augment the direct impact of CO_2 on phytoplankton growth in a biogeochemical model, Elementa: Science of the Anthropocene, 10, https://doi.org/10.1525/elementa.2021.00104, 00104, 2022.

Seifert, M., Danek, C., Völker, C., and Hauck, J.: Model data for "Interactions between ocean alkalinity enhancement and phytoplankton in an Earth System Model", Figshare, https://figshare.com/s/f8dcd2ad0eb8b2c7b137, 2025.

Semmler, T., Danilov, S., Gierz, P., Goessling, H. F., Hegewald, J., Hinrichs, C., Koldunov, N., Khosravi, N., Mu, L., Rackow, T., Sein, D. V., Sidorenko, D., Wang, Q., and Jung, T.: Simulations for CMIP6 with the AWI Climate Model AWI-CM-1-1, Journal of Advances in Modeling Earth Systems, 12, e2019MS002 009, https://doi.org/10.1029/2019MS002009, 2020.

Smith, S. M., Geden, O., Gidden, M. J., Lamb, W. F., Nemet, G. F., Minx, J. C., Buck, H., Burke, J., Cox, E., Edwards, M. R., Fuss, S., Johnstone, I., Müller-Hansen, F., Pongratz, J., Probst, B. S., Roe, S., Schenuit, F., Schulte, I., and Vaughan, N. E.: The State of Carbon Dioxide Removal - 2nd Edition, Tech. rep., https://doi.org/10.17605/OSF.IO/F85QJ, 2024.

Stanmore, B. R. and Gilot, P.: Review–calcination and carbonation of limestone during thermal cycling for CO_2 sequestration, Fuel Processing Technology, 86, 1707–1743, https://doi.org/10.1016/j.fuproc.2005.01.023, 2005.

Stevens, B., Giorgetta, M., Esch, M., Mauritsen, T., Crueger, T., Rast, S., Salzmann, M., Schmidt, H., Bader, J., Block, K., Brokopf, R., Fast, I., Kinne, S., Kornblueh, L., Lohmann, U., Pincus, R., Reichler, T., and Roeckner, E.: Atmospheric component of the MPI-M Earth System Model: ECHAM6, Journal of Advances in Modeling Earth Systems, 5, 146–172, https://doi.org/https://doi.org/10.1002/jame.20015, 2013.

Subhas, A. V., Marx, L., Reynolds, S., Flohr, A., Mawji, E. W., Brown, P. J., and Cael, B. B.: Microbial ecosystem responses to alkalinity enhancement in the North Atlantic Subtropical Gyre, Frontiers in Climate, 4, https://doi.org/10.3389/fclim.2022.784997, 2022.

Suitner, N., Faucher, G., Lim, C., Schneider, J., Moras, C. A., Riebesell, U., and Hartmann, J.: Ocean alkalinity enhancement approaches and the predictability of runaway precipitation processes: results of an experimental study to determine critical alkalinity ranges for safe and sustainable application scenarios, Biogeosciences, 21, 4587–4604, https://doi.org/10.5194/bg-21-4587-2024, 2024.

Sánchez, N., Goldenberg, S. U., Brüggemann, D., Jaspers, C., Taucher, J., and Riebesell, U.: Plankton food web structure and productivity under ocean alkalinity enhancement, Science Advances, 10, eado0264, https://doi.org/10.1126/sciadv.ado0264, 2024.

UNFCCC: United Nations Framework Convention on Climate Change: Paris Agreement, retrieved from https://unfccc.int/sites/default/files/english_paris_agreement.pdf, 08/01/2025, 2015.

Wang, Q., Danilov, S., Sidorenko, D., Timmermann, R., Wekerle, C., Wang, X., Jung, T., and Schröter, J.: The Finite Element Sea Ice-Ocean Model (FESOM) v.1.4: formulation of an ocean general circulation model, Geoscientific Model Development, 7, 663–693, https://doi.org/10.5194/gmd-7-663-2014, 2014.

Wolf-Gladrow, D. and Riebesell, U.: Diffusion and reactions in the vicinity of plankton: A refined model for inorganic carbon transport, Marine Chemistry, 59, 17–34, https://doi.org/https://doi.org/10.1016/S0304-4203(97)00069-8, 1997.

Zeebe, R. E. and Wolf-Gladrow, D.: CO_2 in seawater: Equilibrium, kinetics, isotopes, 65, Gulf Professional Publishing, 2001.